https://doi.org/10.5194/egusphere-2026-382
Preprint. Discussion started: 29 January 2026

An energetic perspective on the impact of the Atlantic Multidecadal Variability on the West African Monsoon

Elsa Mohino[1], Paul-Arthur Monerie[2], Juliette Mignot[3], and Simona Bordoni[4,5]

[1]Departamento de Física de la Tierra y Astrofísica, Universidad Complutense de Madrid, 28040 Madrid, Spain
[2]National Centre for Atmospheric Sciences, University of Reading, Department of Meteorology, P.O. Box 243, Earley Gate, Reading RG6 6BB, UK
[3]LOCEAN/IPSL, IRD/Sorbonne Université/CNRS/MNHN, 4 Place Jussieu, 75005 Paris, France
[4]Department of Civil, Environmental and Mechanical Engineering, University of Trento, I-38123 Trento, Italy
[5]Center Agriculture Food Environment (C3A), University of Trento, San Michele all'Adige, Italy

Correspondence: Elsa Mohino (emohino@ucm.es)

Abstract. This study explores mechanisms by which the Atlantic Multidecadal Variability (AMV) drives multidecadal changes in the West African Monsoon (WAM), with a focus on Sahel rainfall. We investigate this connection through an energetic perspective using atmosphere-ocean coupled models forced by an idealized AMV sea surface temperature (SST) pattern. Results show that a positive AMV phase (warmer North Atlantic) increases net energy input to the atmosphere via enhanced surface latent heat flux. The atmospheric circulation adjusts by exporting this excess energy from the North Atlantic. In the Tropical Atlantic and Africa, this is accomplished by anomalous southward cross-equatorial energy transport and a northward shift of the Intertropical Convergence Zone (ITCZ). Over West Africa, this ITCZ shift leads to increased and northward displaced Sahel rainfall. The monsoon intensification is dynamically consistent with enhanced low-level convergence and high-level divergence in the main ascent region and a decrease in mid-level dry-air intrusion, linked to a weakening of the shallow meridional circulation over the Sahara.

1 Introduction

The West African monsoon (WAM) is a complex, strongly coupled system involving the atmosphere, ocean, and land. Its seasonal cycle is marked by a pronounced northward migration of the associated rainfall, which reaches its northernmost position during July, August, and September (JAS) (Thorncroft et al., 2011). During these months, the semi-arid Sahel region records most of its annual precipitation (Nicholson, 2013). Hence, summer seasonal amounts of Sahel precipitation are closely tied to the strength and latitudinal migrations of the WAM.

Rainfall over the Sahel has experienced strong variability during the instrumental record (Rodríguez-Fonseca et al., 2015), with a notable component at decadal-to-multidecadal timescales (Kitoh et al., 2020). The transition from the rainy years in the 1950s–1960s to the severe drought conditions of the 1970s–1980s was particularly remarkable (Dai et al., 2004). Since then, Sahel rainfall has shown a recovery, accompanied by an increased frequency and intensity of extreme rainfall events (e.g.

https://doi.org/10.5194/egusphere-2026-382
Preprint. Discussion started: 29 January 2026

Sanogo et al., 2015; Taylor et al., 2017; Chagnaud et al., 2022). Regionally, the recovery has been weaker in the western Sahel compared to the central and eastern sectors (Lebel and Ali, 2009).

There is no clear consensus on the ultimate causes of this observed decadal variability in Sahel rainfall in the instrumental period. Changes in external forcings, compounded with internal climate variability, make attribution of these rainfall fluctuations particularly challenging. The limited length of the observational record and systematic biases in climate models further complicate the task (Herman et al., 2023). Consequently, the extent to which the Sahel drought and its subsequent partial recovery can be attributed to anthropogenic influences, such as greenhouse gas emissions or aerosol loads, either through direct or ocean-mediated influences, or to internally generated sea surface temperature (SST) variability, either due to the system's stochasticity or to modifications in the deep oceans, is still highly debated (Rotstayn and Lohmann, 2002; Knight et al., 2006; Haywood et al., 2013; Hwang et al., 2013; Dong et al., 2014; Dong and Sutton, 2015; Hua et al., 2019; Zhang et al., 2019; Moreno-Chamarro et al., 2020; Watanabe and Tatebe, 2019; Giannini and Kaplan, 2019; Hirasawa et al., 2020, 2022; Kim et al., 2020; Zhang et al., 2021, 2022; Ndiaye et al., 2022; He et al., 2023; Herman et al., 2023; Monerie et al., 2023; Guo et al., 2024).

Despite this lack of consensus, there is broad agreement that SST variability associated with the Atlantic Multidecadal Variability (AMV) played a prominent role in modulating Sahel rainfall at decadal timescales. Between 40 and 65% of Sahel rainfall variability at these timescales can in fact be explained by AMV (Zhang and Delworth, 2006; Villamayor et al., 2018; Kitoh et al., 2020; Joshi et al., 2022). Observational and modelling studies consistently show that the positive phase of AMV, characterized by warmer-than-normal SSTs in the North Atlantic and cooler and weaker anomalies in the South Atlantic (Zhang et al., 2019), promotes enhanced rainfall over the Sahel and higher occurrence of extreme rainfall events (Folland et al., 1986; Knight et al., 2006; Zhang and Delworth, 2006; Mohino et al., 2011; Ting et al., 2011; Martin et al., 2014; Martin and Thorncroft, 2014; O'Reilly et al., 2017; Villamayor et al., 2018; Monerie et al., 2019b; Moreno-Chamarro et al., 2020; Hodson et al., 2022; Badji et al., 2022; Mohino et al., 2024; Cai et al., 2025).

Regarding the involved mechanisms, most studies agree that the AMV positive phase shifts the ITCZ northwards and enhances southwesterly surface winds into the Sahel, promoting enhanced low-level moisture flux convergence, convection, and upper-level divergence (Folland et al., 1986; Knight et al., 2006; Zhang and Delworth, 2006; Ting et al., 2011; Mohino et al., 2011; Wang et al., 2012; Zhang et al., 2021). The cross-equatorial winds are also understood as a response to the sea level pressure interhemispheric gradient that follows the interhemispheric SST gradient (Martin et al., 2014; Martin and Thorncroft, 2014; Xue et al., 2022). Both dynamical and thermodynamical changes contribute to the total response of the WAM's precipitation to AMV (O'Reilly et al., 2017; Monerie et al., 2019b). However, there is less agreement on the role of the Saharan Heat Low (SHL) and the shallow meridional circulation (SMC) over the Sahara. While Martin and Thorncroft (2014) suggest that a positive AMV increases Sahel precipitation through an increased SMC in response to a stronger SHL, Shekhar and Boos (2017) challenge this view, highlighting that a strengthened SMC can weaken the monsoon by advecting dry air at mid levels.

The emerging paradigm of monsoons as energetically direct moist circulations, tightly coupled to the ITCZ and the Hadley circulation (Schneider et al., 2014; Biasutti et al., 2018), provides a framework to explore WAM variability from an energetic perspective. The column-integrated moist static energy (MSE) budget offers insights into the WAM response to climate change

https://doi.org/10.5194/egusphere-2026-382
Preprint. Discussion started: 29 January 2026

(Hill et al., 2017, 2018; Mutton et al., 2022). Furthermore, the established relationship between inter-hemispheric atmospheric energy transport and the ITCZ position (Marshall et al., 2014; Donohoe et al., 2014; Bischoff and Schneider, 2014; Schneider et al., 2014; Adam et al., 2016a, b) enables the use of energetic-based metrics to diagnose the location of the monsoon-related rainfall band (Shekhar and Boos, 2016) and to explore uncertainties related to aerosol forcing in understanding 20th-century Sahel rainfall trends (Monerie et al., 2023). The recent extension of this theory to consideration of the influence of proximal deserts on monsoonal precipitation (Shekhar and Boos, 2016) holds promise to also shed light on the SMC-Sahel rainfall relationship in a unified framework.

Motivated by this perspective, the aim of this study is to improve understanding of the impact of AMV on the WAM through the lens of the energetic framework. The limited length of the observational record, the misrepresentation of Sahel multidecadal variability in current reanalyses (Berntell et al., 2018), and the influence of other sources of decadal SST variability, particularly those centred in the Pacific basin (Mohino et al., 2011; Villamayor and Mohino, 2015; Dong and Dai, 2015; Joshi et al., 2022), hinder the evaluation of the AMV influence on the WAM from observations alone. To overcome these limitations, here we adopt a modelling approach in which atmosphere-ocean coupled models are forced with an idealised North Atlantic SST pattern characteristic of the AMV through flux adjustment (Boer et al., 2016). This approach allows us to analyse a large ensemble of realisations, improving signal detection, and to quantify model uncertainty by applying a consistent constraint across different models.

2 Data and methods

2.1 Description of the simulations

We use two sets of sensitivity experiments, consisting of 10-year runs with global coupled models in which North Atlantic SSTs are restored to follow a fixed, idealised anomalous pattern of the AMV in its positive (AVM^{+}) and negative (AVM^{-}) phases, respectively, based on observations (Boer et al., 2016). Four models follow the protocol of the Decadal Climate Prediction Project - Component C (DCPP-C Boer et al., 2016), while nine others follow the protocol proposed in the EU Horizon 2020 PRIMAVERA project (Hodson et al., 2022). In both cases, for each model, multiple ensemble members are generated by slightly perturbing initial conditions. The protocols differ in the applied radiative forcing (pre-industrial conditions in the DCPP-C protocol and 1950s conditions in the PRIMAVERA protocol) and in the magnitude of the anomalous AMV pattern, which is twice as large in the PRIMAVERA runs. Changes associated with a positive AMV phase are estimated by subtracting the negative experiment from the positive one ($AMV^{+} - AMV^{-}$). To facilitate comparison between protocols, changes in the model driven by the PRIMAVERA protocol are halved. For each experiment, we first calculate the 10-year mean of the simulation, and then we average all ensemble members for each model. Since this estimation assumes linearity, the changes associated with a negative AMV phase can be obtained by reversing the sign of the anomalies. The climatology for a given model and field is computed as half the sum of the positive and negative experiments, after averaging across ensemble members and the ten simulated years. Although there could be non-linear effects in the AMV impacts (e.g. Monerie et al., 2019b, 2025), the current protocol does not allow their estimation.

https://doi.org/10.5194/egusphere-2026-382
Preprint. Discussion started: 29 January 2026

Table 1 lists the models analysed, including their atmospheric horizontal resolution, protocol followed, number of ensemble members, and main reference.

2.2 Derived variables

Over the West African Monsoon, the contribution of transient eddies to the time-mean column-integrated energy balance of the atmosphere is small (Hill et al., 2017), allowing the use of monthly mean fields. From the model's monthly mean outputs, we calculate the following derived variables:

- **Top-of-atmosphere radiative energy imbalance:** The energy imbalance at the top of the atmosphere R_{TOA} is calculated as the difference between net incoming shortwave radiation and outgoing longwave radiation (OLR), with positive values indicating net radiative energy gain for the atmosphere.
- **Surface energy imbalance:** The surface energy imbalance F_{SFC} is calculated as the sum of net surface shortwave radiation, net surface longwave radiation, and surface turbulent enthalpy fluxes (latent and sensible heat), with positive values indicating an energy gain for the atmosphere from below.
- **Net energy input:** The net energy input NEI into the atmospheric column is calculated as the sum of the top-of-the-atmosphere and surface energy imbalances. A positive value indicates a net input of energy into the atmosphere.
- **Moist static energy:** Moist static energy (MSE, h) is calculated as $h = c_pT + L_vq + gz$, where c_p is the specific heat at constant pressure, T is the temperature, L_v is the latent heat of vaporization, q is the specific humidity, g is the gravitational constant, and z is the geopotential height.
- **Divergent moist static energy flux:** To estimate the column-integrated divergent MSE flux (inclusive of mean and transient and stationary eddies, $\langle \boldsymbol{u}h \rangle^+$, with $\boldsymbol{u}$ denoting the horizontal wind, brackets the mass-weighted vertical integrals, and $^+$ the divergent component), we use the column-integrated energy balance of the atmosphere:

$$\partial_t \langle e \rangle + \nabla_h \cdot \langle \boldsymbol{u}h \rangle = NEI \tag{1}$$

  where $\partial_t \langle e \rangle$, the time tendency of the mass-weighted vertical integral of moist enthalpy $e = c_pT + L_vq$, represents the moist energy stored in the atmospheric column, and ∇_h is the horizontal divergence operator. Assuming that energy storage is negligible over seasonal and long-term averages (denoted by overbars), we obtain $\nabla_h \cdot \langle \overline{\boldsymbol{u}h} \rangle = \overline{NEI}$. The divergent component of the mass-weighted vertical integral of the MSE flux is hence inferred from NEI assuming the energy budget in Eq. 1 is closed and atmospheric energy storage is negligible.
- **Low-level atmospheric thickness:** We calculate the low-level atmospheric thickness (LLAT) as the difference between the geopotential heights of the 700-hPa and the 950-hPa surfaces as a metric of the Saharan heat low (Shekhar and Boos, 2017). To focus on robust geopotential changes, we remove the tropical mean between 23ºS and 23ºN. Following Shekhar and Boos (2017), we also estimate the value and the latitude of the LLAT maximum using cubic-spline interpolation of the zonally averaged field between 10ºE and 35ºE.

https://doi.org/10.5194/egusphere-2026-382
Preprint. Discussion started: 29 January 2026

- **ITCZ position:** We estimate the zonally varying latitude of the ITCZ, ϕ_{max}, following Adam et al. (2016b) as the position of the maximum rainfall by weighting for each longitude the latitude (ϕ) by the 10th power of the area-weighted precipitation (P) and integrating between 20ºS and 20ºN:

$$\phi_{max} = \frac{\int_{20^\circ S}^{20^\circ N} \phi[\cos(\phi)P]^{10} d\phi}{\int_{20^\circ S}^{20^\circ N} [\cos(\phi)P]^{10} d\phi}$$

- **African Easterly Jet position:** The peak of the African Easterly Jet (AEJ) is identified as the minimum of the 600-hPa zonal wind, zonally averaged between 10ºW and 10ºE, after cubic-spline interpolation.

2.3 Multimodel averaging

To highlight the average signals across models, the multimodel mean is calculated as the unweighted average across all available models (an equal weight "1 model, 1 vote" approach), without any special weighting for different versions of the same model. In this calculation, each model is represented by the average over all its ensemble members, which varies among models (table 1). Before averaging, all model outputs are regridded to a common horizontal grid of 1º × 1º using a first-order conservative method. For the calculation of vertical profiles, outputs are first computed for each model, regridded linearly to a common 1º horizontal grid (vertical levels are standardised, except for EC-Earth3 in the DCPP-C protocol, which is excluded for profile calculations), and then averaged across the available models.

In maps and spatial plots, model consistency is evaluated by hatching the regions where less than 80% of the models agree on the sign of the AMV^+ minus AMV^- changes in a given variable.

2.4 Statistical confidence and intermodel spread

As is common in modelling studies, the intermodel spread is used as a measure of uncertainty. We assume the model values form a sample drawn from a normal distribution with unknown variance, and we use the sample variance as an estimate of the population variance. Confidence intervals are constructed using a two-tailed Student's t-test at a significance level of $\alpha = 0.05$.

We also evaluate the potential relation between the intermodel spread of Sahel rainfall and that of other variables using scatter plots, for which the linear regression and correlation are calculated. The statistical significance of the latter is assessed using a t-test at the same significance level of $\alpha = 0.05$.

Due to the interdependence among models, determining the number of degrees of freedom in our sample of models is not straightforward (Sanderson et al., 2015). Specifically, two elements are provided by the same model (CNRM-CM6-1) run under the two different protocols, while others represent a single model configuration run at different resolutions (for instance, MetUM-GOML2-HR and MetUM-GOML2-LR). Moreover, several models share components (e.g., atmospheric or oceanic), thus reducing overall diversity. Most results shown are based on a sample of 11 models, of which around 6 can be considered independent, although their components might not be completely independent. Therefore, we assess the statistical significance under two assumptions: (1) treating all models as independent realisations, and (2) assuming only 6 independent elements. This dual approach allows us to evaluate the sensitivity of our conclusions to model interdependence. These are indicated in the text and figures with one and two asterisks, respectively.

https://doi.org/10.5194/egusphere-2026-382
Preprint. Discussion started: 29 January 2026

2.5 Symmetric and antisymmetric components of changes

To quantify how much of a given change in a zonally averaged field can be interpreted as a latitudinal shift vs an amplitude change, we decompose anomalies into symmetric and antisymmetric components relative to the location of the climatological peak. We restrict the analysis to zonally averaged (in the 10ºW–10ºE longitudinal sector) fields that exhibit a distinct extremum (maximum or minimum) as a function of latitude (e.g., rainfall or zonal wind at 600 hPa) and focus on a latitude window centred on this peak. For any latitude within this window, the symmetric (antisymmetric) component is defined as half the sum (difference) of the value at that latitude and the value at its mirror latitude relative to the peak. For a given latitude range to one side of the peak (for instance, Sahel latitudes for rainfall), we identify the shift with the antisymmetric component and the amplitude change with the symmetric component, both averaged over the latitude range. The total averaged change for that given latitude range is the sum of both components. Unless otherwise stated, the region taken for the averages is from the latitude of the maximum to the northern limit of the plot. For the multimodel mean, the calculation is performed after model averaging.

3 Results

3.1 Drift in the global energy response and model selection

We evaluate the stability of the simulations by calculating the drift in the TOA energy imbalance R_{TOA} over the simulated years (Fig. 1a). All models except for MPI-ESM-2-HR and MPI-ESM-2-XR show negative R_{TOA}, indicating that the AMV$^+$ experiment is losing energy at TOA relative to AMV$^-$. Although the negative values tend to grow over time, the trends are not statistically significant. This weak negative R_{TOA} and its trend in the difference between AMV$^+$ and AMV$^-$ experiments are consistent with a positive value and trend in OLR (Fig. 1b) and in global mean surface temperatures (Fig. 1c). The flux restoring imposes warm anomalies over the North Atlantic in the AMV$^+$ experiment relative to AMV$^-$, resulting in a warmer global mean surface temperature anomaly (Fig. 1c). This initial anomaly tends to increase over time as regions remote from the North Atlantic begin warming up (Fig. 1c). Consequently, the warmer AMV$^+$ experiment loses more OLR to space relative to the AMV$^-$ experiment (Fig. 1b), which explains the negative R_{TOA} and its weak negative trend (Fig. 1a).

Conversely, MPI-ESM-2-HR and MPI-ESM-2-XR exhibit highly anomalous behaviour. In response to warm North Atlantic SST anomalies, these models cool over the simulated period, especially over the tropical ocean regions (Fig. 1d). The reasons for this cooling remain unclear, and while we encourage further analysis, it is out of the scope of this study. This cooling causes a strong positive drift of R_{TOA} (Fig. 1a) due to a corresponding negative drift in OLR (Fig. 1b). In addition, these models present a strong drift in Sahel rainfall, characterised by a positive and statistically significant trend throughout the simulation (Fig. 1e). We consider this behaviour unrealistic and have therefore removed these two models from the analyses shown here. We caution against the inclusion of the PRIMAVERA AMV$^+$ and AMV$^-$ simulations performed with these two models in multimodel means, as it can unrealistically distort results and increase intermodel spread (as in Hodson et al., 2022).

https://doi.org/10.5194/egusphere-2026-382
Preprint. Discussion started: 29 January 2026

Nevertheless, our main conclusions regarding the mechanisms governing the Sahel rainfall response to the AMV SST pattern remain robust regardless of the exclusion of these two models.

3.2 Changes in Sahel rainfall

In response to the imposed positive AMV pattern during boreal summer, there is a pronounced surface warming across continental regions poleward of 30ºN, including eastern Asia. In the Southern Hemisphere, warm anomalies appear mainly over South America (Fig. 2a). This pattern is consistent with previous studies evaluating similar experiments (Ruprich-Robert et al., 2018, 2021; Monerie et al., 2021; Hodson et al., 2022). Elsewhere, models show weaker and less consistent temperature responses, with modest multimodel mean changes.

In agreement with earlier work (e.g. Folland et al., 1986; Knight et al., 2006; Zhang and Delworth, 2006; Mohino et al., 2011; Ting et al., 2011; Martin et al., 2014; Martin and Thorncroft, 2014; Villamayor et al., 2018; Monerie et al., 2019b; Hodson et al., 2022; Mohino et al., 2024), over West Africa, the positive phase of the AMV leads to increased rainfall over the continent, strongest along the western coast, and over the Atlantic north of 5ºN (Fig. 2b). Negative precipitation anomalies occur to the south of the main convective regions. Models show high consistency in the positive rainfall response over the Sahel, but larger uncertainty over the Guinea Gulf coastal regions west of 0ºE (Fig. 2b). On average, models suggest an increase of $0.10 \pm 0.02^{*}/0.03^{**}$ $\mathrm{mm\,day^{-1}}$ in JAS rainfall over the Sahel, corresponding to approximately 5% of the climatological mean.

Increases in Sahel rainfall can arise from an intensification and/or a northward shift of the main rainband. The meridional dipole of precipitation anomalies in Fig. 2b is suggestive of a northward displacement of the ITCZ. Most models indeed show such a northward ITCZ shift over West Africa (Fig. 2c), with a multimodel mean estimate of $0.09 \pm 0.05^{*}/0.08^{**}$ °. Moreover, the intermodel spread in the magnitude of this shift is positively associated with the spread in Sahel rainfall changes, indicating that models simulating a stronger northward ITCZ shift tend to produce larger rainfall increases over the Sahel.

To further evaluate if the rainfall response is better interpreted as an intensification or a latitudinal shift, we decompose rainfall changes averaged in the 10ºW–10ºE longitude sector into symmetric and antisymmetric components relative to the latitude of maximum climatological rainfall (Fig. 3a). For the multimodel mean, 70% of the changes in rainfall over Sahel latitudes are explained by the antisymmetric component (Fig. 3b), supporting a dominant contribution from a northward displacement of the precipitation pattern. At the individual model level, results are more disparate, with five models showing a dominance of the antisymmetric component and four a dominance of the symmetric component, consistent with an intensification of the mean precipitation pattern. The intermodel spread of changes over the Sahel is positively correlated with both components (Fig. 3c-d), which is expected since their sum represents the total change. However, the correlation with the symmetric component is weak and not statistically significant, while it is stronger and statistically significant for the antisymmetric one.

In summary, in response to the positive AVM phase, models simulate an enhancement of Sahel rainfall, arising from both an intensification and a northward shift of the main rainband. The northward displacement dominates the mean response and also helps explain the intermodel spread in total rainfall changes.

https://doi.org/10.5194/egusphere-2026-382
Preprint. Discussion started: 29 January 2026

3.3 Large-scale mechanism driving changes in Sahel rainfall

As shown above, the response of Sahel rainfall to a positive phase of AMV is dominated by a northward shift of the ITCZ. The energetic framework has established a clear link between similar ITCZ shifts and changes in the cross-equatorial atmospheric energy transport (Donohoe et al., 2014; Adam et al., 2016a, b). It is therefore of interest to investigate whether the identified rainfall changes at Sahel longitudes are related to corresponding changes in cross-equatorial energy transport. To this aim, Fig. 4a shows the net energy input (NEI) into the atmosphere and the divergent component of the column-integrated total MSE flux ($\langle \boldsymbol{u}h \rangle^+$, arrows). In response to a positive AMV, a robust anomalous southward cross-equatorial column-integrated MSE flux develops in the Atlantic and along African longitudes ($\langle vh \rangle^+$, with v the meridional wind, Fig. 4b). Such enhanced southward energy transport is typically realised through a northward displacement of the ascending branch of the Hadley circulation (Donohoe et al., 2014). This mechanism is consistent with the simulated ITCZ shift and the associated increase in Sahel rainfall.

At Sahel longitudes (10ºW–10ºE, yellow box in Fig. 4b), the multimodel mean response in the meridional component of the column-integrated divergent MSE flux across the equator is (-1.4±0.4*/0.6**)·10^6 $\mathrm{W\,m^{-1}}$. Combining this with our previous estimate of the mean ITCZ shift at these longitudes yields a displacement of (-6.2±4.2*)·10^{-8} ° per each $\mathrm{W\,m^{-1}}$. When scaled to the entire latitude circle, this corresponds to (-1.6±1.0*)° per PW. This estimate is in close agreement with those reported by Donohoe et al. (2014) for the observed interannual variability of the zonally averaged ITCZ position.

The southward cross-equatorial energy transport arises as a direct response to the enhanced net input of energy into the atmosphere in the North Atlantic (Fig. 4a, shaded). This energy excess cannot be stored locally and results in large-scale atmospheric circulation adjustments that generate the divergent MSE flux seen in Fig. 4a. Decomposition of the NEI excess into individual contributions from TOA and surface energy imbalances (Figs. 4c and d) shows that the main contribution comes from the surface imbalance, which is in turn principally driven by the latent heat flux (Fig. 4e). The mean NEI anomaly in the North Atlantic (see box in Fig. 4c) is 1.5±0.1*/ 0.2** $\mathrm{W\,m^{-2}}$, 85% of which originates from latent heat flux changes.

Regarding the intermodel spread, the scatterplot in Fig. 4f suggests that models with a stronger southward energy transport response also exhibit larger increases in Sahel precipitation. A similar relationship emerges when comparing Sahel rainfall changes with the NEI or surface energy imbalance averaged over the North Atlantic (Fig. 4g,h): models with higher atmospheric energy input through surface fluxes tend to produce stronger southward cross-equatorial energy transport and greater Sahel rainfall anomalies.

To further analyse the changes in surface latent heat flux, we apply the bulk aerodynamic formula (Hartmann, 2016), whereby the latent heat flux (LE) can be expressed as:

$$LE = L_v \, \rho C_{DE} U_r \, q_s \, (1 - RH)$$

where ρ is the air density, C_{DE} is the aerodynamic transfer coefficient for moisture, U_r is the mean wind speed at the standard height, q_s is the saturation specific humidity, and RH is the relative humidity. To a first-order approximation, we expect the relative change in latent heat flux ($\delta LE/LE$, with δLE denoting the AMV$^+$ minus AMV$^-$ anomalies of latent heat flux and LE the estimated climatological value) to be linearly related to the relative change in saturated specific humidity ($\delta q_s/q_s$), to

https://doi.org/10.5194/egusphere-2026-382
Preprint. Discussion started: 29 January 2026

the relative change in mean wind speed ($\delta U_r/U_r$), and to the negative relative change in relative humidity ($-\delta RH/(1-RH)$). In Fig. 5, we present these terms for the surface, except for the wind speed, which is taken at 1000 hPa, and RH, which is calculated with near-surface specific humidity.

In response to the imposed flux restoring, the warm SST anomalies over the North Atlantic (Fig. 2a) lead to an overall increase in saturation specific humidity (Fig. 5b). This would, in isolation, favour enhanced latent heat flux from the surface over the North Atlantic. However, the anomalous spatial patterns in Figs. 5a and 5b differ markedly. Over the tropical north Atlantic, between the equator and 20ºN, where relative changes in q_s are nearly uniform (Fig. 5b), latent heat flux relative anomalies show a dipole (Fig. 5a), with weak and negative values in the tropical Atlantic between 10º and 20ºN and west of 30ºW, and strong and positive values to the south of 10ºN. These differences suggest the influence of feedbacks that modulate the initial response to the imposed SST anomalies (Shekhar and Boos, 2016). Because the atmosphere is decoupled from the ocean within the SST-restored region, such feedbacks must be of atmospheric origin. Specifically, the northward shift of the Atlantic ITCZ following the AMV$^-$ forced energy surplus in the North Atlantic would reduce the northerly winds to the north of the climatological ITCZ (approximately located at 10ºN) and enhance the southerly winds to the south. This yields a dipole in surface wind speed anomalies (negative north of 10°N, positive to the south; Fig. 5c), which in turn suppresses latent heat flux to the north and increases it to the south, consistent with the pattern in Fig. 5a.

In addition, over the North Atlantic subpolar region, changes in relative humidity further enhance latent heat flux into the atmosphere (Fig. 5d). This contribution comes from a reduction in the northwestern Atlantic RH (note the negative sign of the RH term in the bulk formula), as the positive anomaly in near-surface specific humidity (not shown) is smaller than the saturated one. This likely reflects a circulation-driven export of moist air away from the North Atlantic subpolar region, redistributing the excess moisture generated by warmer SSTs.

In summary, our results show that in response to the positive AMV, enhanced turbulent latent heat fluxes from the North Atlantic increase the atmospheric energy input. The excess energy is then exported from the North Atlantic by anomalous atmospheric circulation patterns, which in turn feed back onto the surface fluxes. The resulting steady state is characterised by a southward cross-equatorial energy flux across the Atlantic and African longitudes. This flux is accomplished by a northward shift of the Hadley circulation's ascending branch and is thus associated with a corresponding northward shift of the ITCZ, ultimately leading to enhanced rainfall over the Sahel.

3.4 Changes in the monsoon structure and dynamics

The large-scale responses to the imposed AMV SST anomalies in the North Atlantic indicate modifications of the West African monsoon that extend beyond changes in seasonal rainfall amounts. The main changes in the monsoon circulation are summarised in Fig. 6. Close to the surface, during the positive phase of the AMV, models consistently show a stronger low-level westerly flow that penetrates further north (Fig. 6a). The magnitude of these anomalies is weak, consistent with the models' general underestimation of the AMV's impact on Sahel rainfall (Mohino et al., 2024). Changes in the low-level meridional wind reveal a weakening of the southerly winds south of 13ºN (Fig. 6b), which enhances low-level wind convergence south of 10ºN (Fig. 6c), in the region of mean climatological ascent (Thorncroft et al., 2011; Nicholson, 2013). Positive meridional

https://doi.org/10.5194/egusphere-2026-382
Preprint. Discussion started: 29 January 2026

wind anomalies peak between 15ºN and 20ºN (Fig. 6b), altering the horizontal wind divergent field by weakening and shifting northward the lower branch of the shallow meridional circulation (SMC) (Fig. 6c).

In the upper troposphere, the Tropical Easterly Jet (TEJ) strengthens, accompanied by enhanced northerlies associated with the upper branch of the Hadley cell (Fig. 6a,b). The upper-level horizontal divergence is also enhanced, especially on its northern edge between 10ºN and 15ºN (Fig. 6c), suggesting a strengthening and northward displacement of the main ascent region, consistent with the rainfall anomalies.

In the mid and lower troposphere, the low-level atmospheric thickness anomalies point to an enhanced and northward-shifted Saharan Heat Low (Lavaysse et al., 2010), with positive anomalies north of 20ºN and negative ones to the south (Fig. 6d, and Figs. S1 and S2 in the supplementary material). These negative anomalies are linked to the surface cooling induced by increased soil moisture following increased precipitation (see Fig. S3 in the supplementary material). The resulting surface cooling modifies the meridional temperature gradients, reducing them south of the climatological maximum and strengthening them to the north, which favours a northward shift of the African Easterly Jet (AEJ), consistent with thermal wind balance (Cook, 1999). Indeed, between 800 and 500hPa, cyclonic zonal wind anomalies south of 20ºN indicate a northward shift of the AEJ (Fig. 6a). The AEJ also shows a slight weakening (see Fig. S4 in the supplementary material). At mid levels, the upper branch of the SMC, located between 15ºN and 20ºN and 800-600 hPa (see climatological contours showing divergence in Fig. 6c), shows a consistent weakening across models (see Fig. S5 in the supplementary material). This is reflected in reduced mid-level divergence and a weaker return flow south of 15ºN (orange boxes in Fig. 6b,c).

Regarding the intermodel spread, the scatter plots shown in Fig. 6e-g suggest that the changes at mid levels are strongly related to the changes in Sahel rainfall. Models with stronger rainfall change over the Sahel are also those that show a stronger northward shift of the AEJ (Fig. 6e), possibly mediated by a stronger soil moisture and surface changes (see Fig. S3 in the supplementary material) and a feedback of the rainfall field on the location and intensity of the AEJ (Cook, 1999). In addition, models that exhibit a weaker shallow meridional circulation, characterised by a weaker mid-level return flow and weaker mid-level divergence close to 15ºN, tend to show a stronger rainfall change in the Sahel (Fig. 6gf). Conversely, neither the intermodel spread of the strength nor of the shift of the Saharan Heat Low structure is related to the change in Sahel rainfall (see Fig S1 and S2 in the supplementary material). The intermodel spread in rainfall changes is also not related to the shift of the divergence by the SMC upper branch (see Fig. S5 in the supplementary material).

The preceding analysis suggests, consistent with Shekhar and Boos (2017), a strong coupling between enhanced Sahel rainfall and a weakened return flow of the SMC at mid-levels. Such a weakening reduces the intrusion of dry air into the Sahel, thereby modifying horizontal advection of moist static energy in the region. To further investigate this mechanism, we examine the column-integrated atmospheric energy balance (eq. 1). Taking time averages, again assuming negligible atmospheric energy storage ($\partial_t \langle \overline{e} \rangle \approx 0$) and decomposing the total transport in mean and eddy components, the energy budget can be written as:

$$\overline{NEI} - \langle \overline{\boldsymbol{u}} \cdot \nabla_h \overline{h} \rangle - \langle \overline{\omega} \partial_p \overline{h} \rangle - \langle \nabla_h (\overline{\boldsymbol{u}' h'}) \rangle = 0$$

where overbars denote time averages, primes denote deviations from the time averages, and ω is the vertical velocity in pressure coordinates. In most deep convective regions, including monsoon systems, the transient eddy term is small and the dominant

https://doi.org/10.5194/egusphere-2026-382
Preprint. Discussion started: 29 January 2026

balance is between positive $\overline{NEI}$ and the MSE divergence by the vertical advection term ($-\langle\overline{\omega}\partial_p\overline{h}\rangle < 0$). In the Sahel monsoon, as shown by Hill et al. (2017), the horizontal advection term ($-\langle\overline{\boldsymbol{u}}\cdot\nabla_h\overline{h}\rangle < 0$) is non negligible and in fact partly balances the positive $\overline{NEI}$ through import of dry, and hence lower MSE, air in the upper branch of the SMC.

Building on these ideas, in Fig. 7, we examine changes in the MSE export by the time-mean horizontal flow ($\overline{\boldsymbol{u}}\cdot\nabla_h\overline{h}$) over the Sahel. Climatologically, the export of MSE at mid-levels is dominated by the moisture advection term ($\overline{\boldsymbol{u}}\cdot\nabla_h L_v\overline{q}$, compare black and blue lines in Fig. 7a), due to northerly flow between 800 hPa and 300 hPa (Fig. 6b) acting on a negative meridional moisture gradient (Fig. 7c, $\partial_y\overline{q}$, blue line and axis), that is, by dry air advection by the upper branch of the SMC, in agreement with Hill et al. (2017). Temperature advection slightly counteracts this MSE export (Fig. 7a, $\overline{\boldsymbol{u}}\cdot\nabla_h c_p\overline{T}$, red line), since the same northerly flow also advects warmer air.

In response to a positive phase of the AMV, models consistently show a reduction in MSE export at mid-levels due to weaker time-mean horizontal advection (Fig. 7b, $\delta(\overline{\boldsymbol{u}}\cdot\nabla_h\overline{h})$, black line). Because changes in NEI over the Sahel are positive (Fig. 4a) and the transient eddy MSE flux divergence is small (e.g. Hill et al., 2017), this reduced horizontal export must be compensated by enhanced export through the divergent circulation. Consequently the vertical advection term ($-\langle\overline{\omega}\partial_p\overline{h}\rangle$) becomes more negative. Given the tropical MSE vertical structure, this implies a change from a shallower convection regime to a deeper convection regime with a first-baroclinic mode structure (Hill et al., 2017). This interpretation agrees with the horizontal divergence anomalies in Fig. 6c, which show reduced divergence at mid levels and stronger divergence aloft.

A decomposition of the change in the time-mean horizontal MSE export in a temperature ($\delta(\overline{\boldsymbol{u}}\cdot\nabla_h c_p\overline{T})$), geopotential height ($\delta(\overline{\boldsymbol{u}}\cdot\nabla_h\overline{z})$) and moisture ($\delta(\overline{\boldsymbol{u}}\cdot\nabla_h L_v\overline{q})$) components shows that the moisture advection term dominates (compare black and blue solid lines in Fig. 7b). Part of the reduced dry-air advection, and therefore the weaker MSE export, stems from the weakening of the meridional flow in the upper branch of the SMC (Fig. 7b, $\delta(\overline{\boldsymbol{u}})\cdot\nabla_h L_v\overline{q}$, blue dotted line), as positive meridional wind anomalies (Fig. 6b) act on the climatological negative meridional moisture gradient (Fig. 7c, blue line and axis). However, and consistent with Hill et al. (2017), the dominant contribution arises from thermodynamic changes (Fig. 7b, $\overline{\boldsymbol{u}}\cdot\delta(\nabla_h L_v\overline{q})$, dashed blue line) linked to changes in the moisture field itself. Under a positive AMV phase, and consistent with a stronger and more northward location of the rainfall band, the tropospheric moisture content increases across West Africa, especially at Sahel latitudes, peaking slightly north of 15ºN in the lower troposphere (not shown). This moistening induces an anomalous positive meridional gradient of moisture in the Sahel (Fig. 7c, $\delta(\partial_y\overline{q})$, orange line and axis). The climatological northerlies (contours in Fig. 6b) acting on this anomalous meridional gradient explain the negative values of the $\overline{\boldsymbol{u}}\cdot\delta(\nabla_h L_v\overline{q})$ term in Fig. 7b (blue dashed line).

Regarding intermodel differences, the scatter plots in Fig. 7d-f suggest that changes in Sahel rainfall are strongly linked to mid-tropospheric MSE horizontal advection ($\delta(\overline{\boldsymbol{u}}\cdot\nabla_h\overline{h})$, Fig. 7d), mainly through the thermodynamic moisture advection component ($\overline{\boldsymbol{u}}\cdot\nabla_h\delta(L_v\overline{q})$, Fig. 7f). Models exhibiting a stronger reduction in MSE export, through a greater decrease in dry air intrusion at mid levels (mainly mediated by modifications in the moisture profile), also simulate larger increases in Sahel rainfall. This relationship is consistent with the models that show greater decreases in mid-tropospheric horizontal divergence (Fig. 6f) indicating a weakening of the shallow convection regime.

https://doi.org/10.5194/egusphere-2026-382
Preprint. Discussion started: 29 January 2026

In summary, a positive phase of AMV promotes a northward shift of the main monsoon circulation features, particularly the Saharan Heat Low and the AEJ. It also enhances low-level convergence near 10ºN and divergence aloft, reinforcing the deep convection branch of the monsoon. While also shifting northward, the shallow meridional circulation weakens, reducing the intrusion of dry air into the Sahel main convective region at mid levels. This weakening not only occurs consistently across models but also scales with the magnitude of rainfall increase. The reduced mid-tropospheric dry-air intrusion lowers the MSE export by horizontal advection, which is then compensated by enhanced MSE export through the divergent circulation (Hill et al., 2017), ultimately supporting stronger precipitation. The dominant driver of the reduced horizontal MSE export is the thermodynamic component of the moisture advection, highlighting a strong coupling between moisture and circulation changes in the West African monsoon response to AMV.

4 Discussion

In this work, we have analysed the impact of AMV on the WAM by comparing two sensitivity experiments (AMV^+ and AMV^-) conducted with different models under a common experimental framework. This framework restores the North Atlantic SSTs towards an idealised AMV pattern, which mitigates some of the limitations inherent to observational analyses, such as the short observational record, the co-existence of different sources of multidecadal variability, and the misrepresentation of Sahel multidecadal variability in current reanalyses (Berntell et al., 2018). It also avoids uncertainties associated with model-dependent SST patterns linked to AMV in fully coupled ocean-atmosphere simulations (Martin et al., 2014). Nevertheless, our approach is not exempt from its own limitations.

The SST restoring, imposed in the North Atlantic, effectively decouples the ocean from the atmosphere in that region. Aside from potentially destabilising the climate system in two models (MPI-ESM1-2-HR and MPI-ESM1-2-XR), this decoupling may alter the surface energy exchanges, particularly in the tropical and subtropical North Atlantic (O'Reilly et al., 2023). On the one hand, the positive surface heat flux anomalies shown in Fig. 4d would thermodynamically cool the tropical SSTs, thereby dampening these fluxes. On the other hand, the surface wind anomalies accompanying the northward shift of the ITCZ could also induce dynamical changes in the ocean, potentially altering equatorial upwelling and heat transport via the subtropical cells (Schneider et al., 2014). These ocean-atmosphere feedbacks could influence our estimates of NEI and of the dominant role of surface latent heat fluxes in driving it. Nevertheless, the potential problems of SST restoring for surface heat fluxes in the tropical and subtropical North Atlantic are likely smaller during boreal summer (Kim et al., 2020; O'Reilly et al., 2023), our season of interest. Furthermore, the observed relationship between reduced sea surface salinity, moisture flux divergence, and Sahel multidecadal variability (Li et al., 2016) suggests that surface latent heat fluxes indeed play a relevant role in the observed AMV–WAM coupling.

Contrary to what might be expected if the restored set up resulted in an overestimation of the relevance of tropical North Atlantic SSTs (Kim et al., 2020; O'Reilly et al., 2023), the simulated response to AMV is weak. The low-level zonal wind response in Fig. 6a is approximately ten times weaker than the observational estimates shown by Martin and Thorncroft (2014), which cannot be accounted for by the surface temperature differences to which they are associated (roughly 2-4 times weaker

https://doi.org/10.5194/egusphere-2026-382
Preprint. Discussion started: 29 January 2026

in the simulations with respect to the composite used in Martin and Thorncroft (2014)). The underestimation of the response in WAM circulation is in agreement with the one already identified by Mohino et al. (2024) in the simulated precipitation response and could be due to a lack of forcing. One could argue that part of the multidecadal variability of WAM responds directly to radiative forcings (i.e., it is not ocean mediated, Dong and Sutton, 2015; Hirasawa et al., 2020), and hence is absent from our experiments. Alternatively, as suggested by Herman et al. (2023), if most of WAM's multidecadal variability is indeed ocean mediated, the weak simulated response might indicate that SST anomalies outside the North Atlantic also contribute to the overall AMV impact. Another potential explanation for the weak response is the under-representation of key processes and feedbacks, such as those related to soil moisture (Li et al., 2016), African dust (Wang et al., 2012; Balkanski et al., 2021) or vegetation (Wang et al., 2004), which could also hinder the simulated response of WAM to SST anomalies.

In contrast to Martin and Thorncroft (2014), our results do not support the hypothesis that the positive phase of AMV enhances Sahel rainfall through an intensification of the shallow meridional circulation (SMC) established over the Sahara. While the entire monsoon system shifts northward and the Saharan heat low (SHL) deepens, as indicated by increased low-level atmospheric thickness, the SMC consistently weakens across models (Fig. 6c). This result aligns with the mechanism proposed by Shekhar and Boos (2017). The intermodel comparison highlights the relevant role of this SMC weakening at mid-levels: models showing weaker SMC exhibit larger Sahel rainfall increases in response to the positive phase of AMV. Conversely, there is no clear relationship between any measure (strength or shift) of the SHL and Sahel rainfall intensity (see Figs. S1 and S2 in the supplementary material).

Our results further suggest that, in response to a positive phase of AMV, the increase in Sahel rainfall is associated with a reduction of mid-level dry air intrusion from the north, which reduces the MSE export by the time-mean horizontal flow. This is consistent with a transition to deeper convection and a more top-heavy monsoon structure. This association is in good agreement with recent studies investigating the response of Sahel rainfall to climate change (Mutton et al., 2022, 2024), reinforcing the notion that a weakening of the SMC and a reduction in mid-level dry air intrusion are key features of a wetter Sahel. Interestingly, the dominant driver of this reduced mid-level dry air is the thermodynamic component of the moisture advection, suggesting a strong coupling between moisture and circulation changes.

5 Conclusions

In this study, we analysed simulations from 13 coupled models in which the North Atlantic SSTs were restored to follow an idealised SST pattern representative of the AMV. We compared two experiments, AMV^+ and AMV^-, to estimate the linear response to the AMV and study its impact on the WAM from an energetic perspective. The simulations showed no significant drift, except for two models, whose results were deemed unrealistic and were not included in subsequent analyses.

All models simulate increased Sahel rainfall during the positive AMV phase. The multimodel mean response is best described as a northward shift of the local ITCZ rather than a mere intensification. Intermodel differences in the increase of Sahel rainfall are also positively correlated with those in the northward ITCZ shift.

https://doi.org/10.5194/egusphere-2026-382
Preprint. Discussion started: 29 January 2026

From an energetic perspective, ITCZ shifts, such as those simulated in the Atlantic and West Africa in response to a positive AMV phase, have been associated with changes in the cross-equatorial energy transport (Donohoe et al., 2014; Adam et al., 2016a, b). The imposed warm SST anomalies lead to an increase in the net energy input into the atmosphere over the North Atlantic. This excess energy is then exported from this region by the atmospheric circulation. In the tropical region, such export is directed towards the southern hemisphere, with an anomalous southward cross-equatorial energy flux in Atlantic and African longitudes. As this transport is primarily accomplished by the Hadley circulation (Schneider et al., 2014), the southward cross-equatorial energy flux is consistent with a northward shift of the Atlantic and African ITCZ, leading to enhanced rainfall over the Sahel. Additionally, there is a positive intermodel correlation between anomalous Sahel rainfall and southward cross-equatorial energy flux at Sahel latitudes and net energy input over the North Atlantic. The enhanced NEI into the atmosphere in the North Atlantic arises from enhanced surface latent heat driven by the warmer SST, with feedbacks from the atmospheric circulation further modulating surface fluxes, particularly through wind adjustments accompanying the northward-shifted ITCZ.

The large-scale atmospheric response to the imposed North Atlantic SST anomalies results in coherent changes in the monsoonal circulation consistent with stronger Sahel rainfall. The Saharan heat low and the African Easterly Jet are displaced northward, the low-level southwesterly monsoonal flow is enhanced over the Sahel, and both the low-level wind convergence and the upper-level divergence in the region of main climatological ascent strengthen, indicating a stronger and northward displaced deep convection zone. In agreement with Shekhar and Boos (2017), the shallow meridional circulation over the Sahara and the mid-level dry-air advection into the Sahel are consistently weakened across models. In addition, the reduction in mid-level dry-air intrusion shows a strong positive intermodel correlation with Sahel rainfall increases.

The modelled equilibrium response of the WAM to AMV also suggests a strong feedback between moisture and circulation changes. The response of the AEJ and part of the northward shift of the Saharan heat low can be traced back to modifications in surface temperature, which are themselves related to the modified rainfall response through changes in soil moisture and local surface turbulent fluxes. Moreover, the thermodynamic component of the response, namely enhanced atmospheric moisture throughout the column, further suppresses dry-air intrusion and promotes deeper convection, sustaining the rainfall increase.

Finally, the energetic framework used in this study, linking the NEI into the atmosphere to the divergent component of the vertically integrated MSE flux, proves to be a powerful diagnostic tool for understanding in simple energetic terms the impact of AMV on Sahel rainfall. This framework may also help elucidate other extratropical sources of variability for Sahel rainfall, such as Arctic sea-ice loss and Southern Ocean warming (Monerie et al., 2019a; Jeong et al., 2025; Datti et al., 2025), whose effects are primarily expressed through meridional shifts of the energy transport. For other sources of Sahel decadal variability, such as the Pacific Decadal Variability (Mohino et al., 2011; Villamayor and Mohino, 2015; Dong and Dai, 2015; Joshi et al., 2022), consideration of the zonal component of the vertical integral of MSE flux and associated shifts of the energy flux prime meridian (Boos and Korty, 2016) could provide additional insights.

https://doi.org/10.5194/egusphere-2026-382
Preprint. Discussion started: 29 January 2026

Code and data availability. Data used in this work are publicly available. Model simulations can be downloaded from the Earth System Grid Federation CMIP6 archive (https://esgf-ui.ceda.ac.uk/search, last access: 22 January 2026). The original data has been processed with Climate Data Operators (cdo) (Schulzweida, 2023). The scripts used in this study are available upon reasonable request to the corresponding author.

Author contributions. EM provided the first design of the article, which was subsequently discussed with PAM, JM, and SB. EM did the formal analysis and wrote the original draft. All authors reviewed and edited the paper.

Competing interests. Authors declare no competing interests.

Acknowledgements. Elsa Mohino received funding from the Spanish Ministry of Science and Innovation from DISTROPIA and OFF projects (grant no. PID2021-125806NB-I00 and TED2021-130106B-I00), and the "Recualificación del Sistema Universitario Español para 2021–2023" call from the Universidad Complutense de Madrid, which has been financed by the Ministry of Universities with funds from the Next Generation of the European Union. Simona Bordoni and Elsa acknowledge support from Horizon 2020 project nextGEMS under grant agreement number 101003470. Simona Bordoni also acknowledges support by the Wellcome Trust [project ACCLIMATISE, grant number 308964/Z/23/Z] Authors acknowledge the use of JASMIN facilities for the PRIMAVERA data as part of the IS-ENES3 project that has received funding from the European Union's Horizon 2020 research and innovation program (grant no. 824084). We acknowledge the World Climate Research Programme, which, through its Working Group on Coupled Modelling, coordinated and promoted CMIP6. We thank the climate modelling groups for producing and making available their model output, the Earth System Grid Federation (ESGF) for archiving the data and providing access, and the multiple funding agencies that support CMIP6 and ESGF. This project was provided with computing HPC and storage resources by GENCI at TGCC thanks to the grant 2024-A0170107403 on the supercomputer Joliot Curie's SKL and ROME partition.

https://doi.org/10.5194/egusphere-2026-382
Preprint. Discussion started: 29 January 2026

References

Adam, O., Bischoff, T., and Schneider, T.: Seasonal and Interannual Variations of the Energy Flux Equator and ITCZ. Part I: Zonally Averaged ITCZ Position, Journal of Climate, 29, 3219–3230, https://doi.org/10.1175/JCLI-D-15-0512.1, 2016a.

Adam, O., Bischoff, T., and Schneider, T.: Seasonal and Interannual Variations of the Energy Flux Equator and ITCZ. Part II: Zonally Varying Shifts of the ITCZ, Journal of Climate, 29, 7281–7293, https://doi.org/10.1175/JCLI-D-15-0710.1, 2016b.

Badji, A., Mohino, E., Diakhaté, M., Mignot, J., and Gaye, A. T.: Decadal Variability of Rainfall in Senegal: Beyond the Total Seasonal Amount, Journal of Climate, 35, 5339–5358, https://doi.org/10.1175/JCLI-D-21-0699.1, 2022.

Balkanski, Y., Bonnet, R., Boucher, O., Checa-Garcia, R., and Servonnat, J.: Better representation of dust can improve climate models with too weak an African monsoon, Atmospheric Chemistry and Physics, 21, 11 423–11 435, https://doi.org/10.5194/acp-21-11423-2021, 2021.

Berntell, E., Zhang, Q., Chafik, L., and Körnich, H.: Representation of multidecadal Sahel rainfall variability in 20th century reanalyses, Scientific reports, 8, 10 937, https://doi.org/10.1038/s41598-018-29217-9, 2018.

Biasutti, M., Voigt, A., Boos, W. R., Braconnot, P., Hargreaves, J. C., Harrison, S. P., Kang, S. M., Mapes, B. E., Scheff, J., and Schumacher, C.: Global energetics and local physics as drivers of past, present and future monsoons, Nature Geoscience, 11, 392–400, https://doi.org/10.1038/s41561-018-0137-1, 2018.

Bischoff, T. and Schneider, T.: Energetic constraints on the position of the intertropical convergence zone, Journal of Climate, 27, 4937–4951, https://doi.org/10.1175/JCLI-D-13-00650.1, 2014.

Boer, G. J., Smith, D. M., Cassou, C., Doblas-Reyes, F., Danabasoglu, G., Kirtman, B., Kushnir, Y., Kimoto, M., Meehl, G. A., Msadek, R., Mueller, W. A., Taylor, K. E., Zwiers, F., Rixen, M., Ruprich-Robert, Y., and Eade, R.: The Decadal Climate Prediction Project (DCPP) contribution to CMIP6, Geoscientific Model Development, 9, 3751–3777, https://doi.org/10.5194/gmd-9-3751-2016, 2016.

Boos, W. R. and Korty, R. L.: Regional energy budget control of the intertropical convergence zone and application to mid-Holocene rainfall, Nature Geoscience, 9, 892–897, https://doi.org/10.1038/ngeo2833, 2016.

Boucher, O., Servonnat, J., Albright, A. L., Aumont, O., Balkanski, Y., Bastrikov, V., Bekki, S., Bonnet, R., Bony, S., Bopp, L., Braconnot, P., Brockmann, P., Cadule, P., Caubel, A., Cheruy, F., Codron, F., Cozic, A., Cugnet, D., D'Andrea, F., Davini, P., de Lavergne, C., Denvil, S., Deshayes, J., Devilliers, M., Ducharne, A., Dufresne, J.-L., Dupont, E., Ethe, C., Fairhead, L., Falletti, L., Flavoni, S., Foujols, M.-A., Gardoll, S., Gastineau, G., Ghattas, J., Grandpeix, J.-Y., Guenet, B., Guez, L. E., Guilyardi, E., Guimberteau, M., Hauglustaine, D., Hourdin, F., Idelkadi, A., Joussaume, S., Kageyama, M., Khodri, M., Krinner, G., Lebas, N., Levavasseur, G., Levy, C., Li, L., Lott, F., Lurton, T., Luyssaert, S., Madec, G., Madeleine, J.-B., Maignan, F., Marchand, M., Marti, O., Mellul, L., Meurdesoif, Y., Mignot, J., Musat, I., Ottle, C., Peylin, P., Planton, Y., Polcher, J., Rio, C., Rochetin, N., Rousset, C., Sepulchre, P., Sima, A., Swingedouw, D., Thieblemont, R., Traore, A. K., Vancoppenolle, M., Vial, J., Vialard, J., Viovy, N., and Vuichard, N.: Presentation and Evaluation of the IPSL-CM6A-LR Climate Model, Journal of Advances in Modeling Earth Systems, 12, e2019MS002 010, https://doi.org/10.1029/2019MS002010, 2020.

Cai, W., Reason, C., Mohino, E., Rodríguez-Fonseca, B., Malherbe, J., Santoso, A., Li, X., Chikoore, H., Nnamchi, H., McPhaden, M. J., Keenlyside, N., Taschetto, A. S., Wu, L., Ng, B., Liu, Y., Geng, T., Yang, K., Wang, G., Jia, F., Lin, X., Li, S., Yang, Y., Wang, J., Zhang, L., Li, Z., Wilfried, P., Zhou, L., Zhang, X., Engelbrecht, F., Li, Z., and Mutemi, J. N.: Climate impacts of the El Niño–Southern Oscillation in Africa, Nature Reviews Earth & Environment, 6, 503–520, https://doi.org/10.1038/s43017-025-00705-7, 2025.

Chagnaud, G., Panthou, G., Vischel, T., and Lebel, T.: A synthetic view of rainfall intensification in the West African Sahel, Environmental Research Letters, 17, 044 005, https://doi.org/10.1088/1748-9326/ac4a9c, 2022.

https://doi.org/10.5194/egusphere-2026-382
Preprint. Discussion started: 29 January 2026

Cook, K. H.: Generation of the African easterly jet and its role in determining West African precipitation, JOURNAL OF CLIMATE, 12, 1165–1184, https://doi.org/10.1175/1520-0442(1999)012<1165:GOTAEJ>2.0.CO;2, 1999.

Dai, A., Lamb, P. J., Trenberth, K. E., Hulme, M., Jones, P. D., and Xie, P.: The recent Sahel drought is real, International Journal of climatology, 24, 1323–1331, 2004.

Datti, A. D., Zeng, G., Monerie, P.-A., Oo, K. T., and Chen, C.: A Review of the arctic-West African monsoon nexus: How arctic sea ice decline influences monsoon system, Theoretical and Applied Climatology, 156, 9, https://doi.org/10.1007/s00704-024-05255-4, 2025.

Dong, B. and Dai, A.: The influence of the Interdecadal Pacific Oscillation on Temperature and Precipitation over the Globe, Climate Dynamics, 45, 2667–2681, https://doi.org/10.1007/s00382-015-2500-x, 2015.

Dong, B. and Sutton, R.: Dominant role of greenhouse-gas forcing in the recovery of Sahel rainfall, Nature Climate Change, 5, 757–U173, https://doi.org/10.1038/NCLIMATE2664, 2015.

Dong, B., Sutton, R. T., Highwood, E., and Wilcox, L.: The impacts of European and Asian anthropogenic sulfur dioxide emissions on Sahel rainfall, Journal of Climate, 27, 7000–7017, https://doi.org/10.1175/JCLI-D-13-00769.1, 2014.

Donohoe, A., Marshall, J., Ferreira, D., Armour, K., and McGee, D.: The Interannual Variability of Tropical Precipitation and Interhemispheric Energy Transport, Journal of Climate, 27, 3377–3392, https://doi.org/10.1175/JCLI-D-13-00499.1, 2014.

Döscher, R., Acosta, M., Alessandri, A., Anthoni, P., Arsouze, T., Bergman, T., Bernardello, R., Boussetta, S., Caron, L.-P., Carver, G., Castrillo, M., Catalano, F., Cvijanovic, I., Davini, P., Dekker, E., Doblas-Reyes, F. J., Docquier, D., Echevarria, P., Fladrich, U., Fuentes-Franco, R., Gröger, M., v. Hardenberg, J., Hieronymus, J., Karami, M. P., Keskinen, J.-P., Koenigk, T., Makkonen, R., Massonnet, F., Ménégoz, M., Miller, P. A., Moreno-Chamarro, E., Nieradzik, L., van Noije, T., Nolan, P., O'Donnell, D., Ollinaho, P., van den Oord, G., Ortega, P., Prims, O. T., Ramos, A., Reerink, T., Rousset, C., Ruprich-Robert, Y., Le Sager, P., Schmith, T., Schrödner, R., Serva, F., Sicardi, V., Sloth Madsen, M., Smith, B., Tian, T., Tourigny, E., Uotila, P., Vancoppenolle, M., Wang, S., Wårlind, D., Willén, U., Wyser, K., Yang, S., Yepes-Arbós, X., and Zhang, Q.: The EC-Earth3 Earth system model for the Coupled Model Intercomparison Project 6, Geoscientific Model Development, 15, 2973–3020, https://doi.org/10.5194/gmd-15-2973-2022, 2022.

Folland, C., Palmer, T., and Parker, D.: Sahel Rainfall and Worldwide Sea Temperatures, 1901-85, Nature, 320, 602–607, https://doi.org/10.1038/320602a0, 1986.

Giannini, A. and Kaplan, A.: The role of aerosols and greenhouse gases in Sahel drought and recovery, Climatic Change, 152, 449–466, https://doi.org/10.1007/s10584-018-2341-9, 2019.

Guo, J., Xie, X., Myhre, G., Shindell, D., Kirkevåg, A., Iversen, T., Samset, B. H., Shi, Z., Li, X., Sun, H., Liu, X., and Liu, Y.: Increased Asian Sulfate Aerosol Emissions Remarkably Enhance Sahel Summer Precipitation, Earth's Future, 12, e2024EF004 745, https://doi.org/10.1029/2024EF004745, 2024.

Gutjahr, O., Putrasahan, D., Lohmann, K., Jungclaus, J. H., von Storch, J.-S., Brüggemann, N., Haak, H., and Stössel, A.: Max Planck Institute Earth System Model (MPI-ESM1.2) for the High-Resolution Model Intercomparison Project (HighResMIP), Geoscientific Model Development, 12, 3241–3281, https://doi.org/10.5194/gmd-12-3241-2019, 2019.

Haarsma, R., Acosta, M., Bakhshi, R., Bretonniere, P.-A., Caron, L.-P., Castrillo, M., Corti, S., Davini, P., Exarchou, E., Fabiano, F., Fladrich, U., Franco, R. F., Garcia-Serrano, J., von Hardenberg, J., Koenigk, T., Levine, X., Meccia, V. L., van Noije, T., van den Oord, G., Palmeiro, F. M., Rodrigo, M., Ruprich-Robert, Y., Le Sager, P., Tourigny, E., Wang, S., van Weele, M., and Wyser, K.: HighResMIP versions of EC-Earth: EC-Earth3P and EC-Earth3P-HR - description, model computational performance and basic validation, Geoscientific Model Development, 13, 3507–3527, https://doi.org/10.5194/gmd-13-3507-2020, 2020.

Hartmann, D. L.: Global physical climatology, Elsevier, Amsterdam, Netherlands, second edn., ISBN 978-0-12-328531-7, 2016.

https://doi.org/10.5194/egusphere-2026-382
Preprint. Discussion started: 29 January 2026

Haywood, J. M., Jones, A., Bellouin, N., and Stephenson, D.: Asymmetric forcing from stratospheric aerosols impacts Sahelian rainfall, Nature Climate Change, 3, 660–665, https://doi.org/10.1038/nclimate1857, 2013.

He, C., Clement, A. C., Kramer, S. M., Cane, M. A., Klavans, J. M., Fenske, T. M., and Murphy, L. N.: Tropical Atlantic multidecadal variability is dominated by external forcing, Nature, 622, 521–527, https://doi.org/10.1038/s41586-023-06489-4, 2023.

Herman, R. J., Biasutti, M., and Kushnir, Y.: Drivers of low-frequency Sahel precipitation variability: comparing CMIP5 and CMIP6 ensemble means with observations, Climate Dynamics, 61, 4449–4470, https://doi.org/10.1007/s00382-023-06755-1, 2023.

Hill, S. A., Ming, Y., Held, I. M., and Zhao, M.: A Moist Static Energy Budget-Based Analysis of the Sahel Rainfall Response to Uniform Oceanic Warming, JOURNAL OF CLIMATE, 30, 5637–5660, https://doi.org/10.1175/JCLI-D-16-0785.1, 2017.

Hill, S. A., Ming, Y., and Zhao, M.: Robust responses of the Sahelian hydrological cycle to global warming, Journal of Climate, 31, 9793–9814, https://doi.org/10.1175/JCLI-D-18-0238.1, 2018.

Hirasawa, H., Kushner, P. J., Sigmond, M., Fyfe, J., and Deser, C.: Anthropogenic Aerosols Dominate Forced Multidecadal Sahel Precipitation Change through Distinct Atmospheric and Oceanic Drivers, Journal of Climate, 33, 10 187–10 204, https://doi.org/10.1175/JCLI-D-19-0829.1, 2020.

Hirasawa, H., Kushner, P. J., Sigmond, M., Fyfe, J., and Deser, C.: Evolving Sahel rainfall response to anthropogenic aerosols driven by shifting regional oceanic and emission influences, Journal of Climate, 35, 3181–3193, https://doi.org/10.1175/JCLI-D-21-0795.1, 2022.

Hirons, L. C., Klingaman, N. P., and Woolnough, S. J.: MetUM-GOML1: a near-globally coupled atmosphere–ocean-mixed-layer model, Geoscientific Model Development, 8, 363–379, https://doi.org/10.5194/gmd-8-363-2015, 2015.

Hodson, D. L. R., Bretonniere, P.-A., Cassou, C., Davini, P., Klingaman, N. P., Lohmann, K., Lopez-Parages, J., Martin-Rey, M., Moine, M.-P., Monerie, P.-A., Putrasahan, D. A., Roberts, C. D., Robson, J., Ruprich-Robert, Y., Sanchez-Gomez, E., Seddon, J., and Senan, R.: Coupled climate response to Atlantic Multidecadal Variability in a multi-model multi-resolution ensemble, Climate Dynamics, 59, 805–836, https://doi.org/10.1007/s00382-022-06157-9, 2022.

Hua, W., Dai, A., Zhou, L., Qin, M., and Chen, H.: An Externally Forced Decadal Rainfall Seesaw Pattern Over the Sahel and Southeast Amazon, Geophysical Research Letters, 46, 923–932, https://doi.org/10.1029/2018GL081406, 2019.

Hwang, Y., Frierson, D. M. W., and Kang, S. M.: Anthropogenic sulfate aerosol and the southward shift of tropical precipitation in the late 20th century, Geophysical Research Letters, 40, 2845–2850, https://doi.org/10.1002/grl.50502, 2013.

Jeong, H., Park, H.-S., Kang, S. M., and Chung, E.-S.: The greater role of Southern Ocean warming compared to Arctic Ocean warming in shifting future tropical rainfall patterns, Nature Communications, 16, 2790, https://doi.org/10.1038/s41467-025-57654-4, 2025.

Joshi, M. K., Rai, A., and Kulkarni, A.: Global-scale interdecadal variability a skillful predictor at decadal-to-multidecadal timescales for Sahelian and Indian Monsoon Rainfall, npj Climate and Atmospheric Science, 5, 2, https://doi.org/10.1038/s41612-021-00227-1, 2022.

Kim, W. M., Yeager, S., and Danabasoglu, G.: Atlantic multidecadal variability and associated climate impacts initiated by ocean thermohaline dynamics, Journal of Climate, 33, 1317–1334, https://doi.org/10.1175/JCLI-D-19-0530.1, 2020.

Kitoh, A., Mohino, E., Ding, Y., Rajendran, K., Ambrizzi, T., Marengo, J., and Magaña, V.: Combined oceanic influences on continental climates, in: Interacting climates of ocean basins: observations, mechanisms, predictability, and impacts, vol. 1, pp. 216–249, 1ed. New York, USA: Cambridge University Press, 2020.

Knight, J. R., Folland, C. K., and Scaife, A. A.: Climate impacts of the Atlantic Multidecadal Oscillation, Geophysical Research Letters, 33, L17 706, https://doi.org/10.1029/2006GL026242, 2006.

Lavaysse, C., Flamant, C., and Janicot, S.: Regional-scale convection patterns during strong and weak phases of the Saharan heat low, Atmospheric Science Letters, 11, 255–264, https://doi.org/https://doi.org/10.1002/asl.284, 2010.

https://doi.org/10.5194/egusphere-2026-382
Preprint. Discussion started: 29 January 2026

Lebel, T. and Ali, A.: Recent trends in the Central and Western Sahel rainfall regime (1990-2007), Journal of Hydrology, 375, 52–64, https://doi.org/10.1016/j.jhydrol.2008.11.030, 2009.

Li, L., Schmitt, R. W., Ummenhofer, C. C., and Karnauskas, K. B.: North Atlantic salinity as a predictor of Sahel rainfall, Science Advances, 2, e1501 588, https://doi.org/10.1126/sciadv.1501588, 2016.

Marshall, J., Donohoe, A., Ferreira, D., and McGee, D.: The ocean's role in setting the mean position of the Inter-Tropical Convergence Zone, Climate Dynamics, 42, 1967–1979, https://doi.org/10.1007/s00382-013-1767-z, 2014.

Martin, E. R. and Thorncroft, C. D.: The impact of the AMO on the West African monsoon annual cycle, Quarterly Journal of the Royal Meteorological Society, 140, 31–46, https://doi.org/10.1002/qj.2107, 2014.

Martin, E. R., Thorncroft, C., and Booth, B. B. B.: The Multidecadal Atlantic SST-Sahel Rainfall Teleconnection in CMIP5 Simulations, Journal of Climate, 27, 784–806, https://doi.org/10.1175/JCLI-D-13-00242.1, 2014.

Mohino, E., Janicot, S., and Bader, J.: Sahel rainfall and decadal to multi-decadal sea surface temperature variability, Climate Dynamics, 37, 419–440, https://doi.org/10.1007/s00382-010-0867-2, 2011.

Mohino, E., Monerie, P.-A., Mignot, J., Diakhaté, M., Donat, M., Roberts, C. D., and Doblas-Reyes, F.: Impact of Atlantic multi-decadal variability on rainfall intensity distribution and timing of the West African monsoon, Earth System Dynamics, 15, 15–40, https://doi.org/10.5194/esd-15-15-2024, 2024.

Monerie, P., Dittus, A. J., Wilcox, L. J., and Turner, A. G.: Uncertainty in Simulating Twentieth Century West African Precipitation Trends: The Role of Anthropogenic Aerosol Emissions, Earth's Future, 11, e2022EF002 995, https://doi.org/10.1029/2022EF002995, 2023.

Monerie, P.-A., Oudar, T., and Sanchez-Gomez, E.: Respective impacts of Arctic sea ice decline and increasing greenhouse gases concentration on Sahel precipitation, Climate Dynamics, 52, 5947–5964, https://doi.org/10.1007/s00382-018-4488-5, 2019a.

Monerie, P.-A., Robson, J., Dong, B., Hodson, D. L. R., and Klingaman, N. P.: Effect of the Atlantic Multidecadal Variability on the Global Monsoon, Geophysical Research Letters, 46, 1765–1775, https://doi.org/10.1029/2018GL080903, 2019b.

Monerie, P.-A., Robson, J., Dong, B., and Hodson, D.: Role of the Atlantic multidecadal variability in modulating East Asian climate, Climate Dynamics, 56, 381–398, https://doi.org/10.1007/s00382-020-05477-y, 2021.

Monerie, P.-A., Mohino, E., Moine, M.-P., Biasutti, M., Pohl, B., and Mignot, J.: Exploring uncertainty in dynamical future changes in Sahel precipitation: the extratropical influence, Climate Dynamics, 63, 1–21, https://doi.org/https://doi.org/10.1007/s00382-025-07835-0, 2025.

Moreno-Chamarro, E., Marshall, J., and Delworth, T. L.: Linking ITCZ migrations to the AMOC and North Atlantic/Pacific SST decadal variability, Journal of Climate, 33, 893–905, https://doi.org/10.1175/JCLI-D-19-0258.1, 2020.

Mutton, H., Chadwick, R., Collins, M., Lambert, F. H., Geen, R., Todd, A., and Taylor, C. M.: The impact of the direct radiative effect of increased CO 2 on the West African monsoon, Journal of Climate, 35, 2441–2458, https://doi.org/10.1175/JCLI-D-21-0340.1, 2022.

Mutton, H., Chadwick, R., Collins, M., Lambert, F. H., Taylor, C. M., Geen, R., and Todd, A.: The impact of a uniform ocean warming on the West African monsoon, Climate Dynamics, 62, 103–122, https://doi.org/10.1007/s00382-023-06898-1, 2024.

Ndiaye, C. D., Mohino, E., Mignot, J., and Sall, S. M.: On the Detection of Externally Forced Decadal Modulations of the Sahel Rainfall over the Whole Twentieth Century in the CMIP6 Ensemble, Journal of Climate, 35, 3339–3354, https://doi.org/10.1175/JCLI-D-21-0585.1, 2022.

Nicholson, S. E.: The West African Sahel: A Review of Recent Studies on the Rainfall Regime and Its Interannual Variability, International Scholarly Research Notices, 2013, e453 521, https://doi.org/10.1155/2013/453521, 2013.

O'Reilly, C. H., Woollings, T., and Zanna, L.: The dynamical influence of the Atlantic multidecadal oscillation on continental climate, Journal of Climate, 30, 7213–7230, https://doi.org/10.1175/JCLI-D-16-0345.1, 2017.

https://doi.org/10.5194/egusphere-2026-382
Preprint. Discussion started: 29 January 2026

O'Reilly, C. H., Patterson, M., Robson, J., Monerie, P. A., Hodson, D., and Ruprich-Robert, Y.: Challenges with interpreting the impact of Atlantic Multidecadal Variability using SST-restoring experiments, Npj Climate and Atmospheric Science, 6, 14, https://doi.org/10.1038/s41612-023-00335-0, 2023.

Roberts, C. D., Senan, R., Molteni, F., Boussetta, S., Mayer, M., and Keeley, S. P. E.: Climate model configurations of the ECMWF Integrated Forecasting System (ECMWF-IFS cycle 43r1) for HighResMIP, Geoscientific Model Development, 11, 3681–3712, https://doi.org/10.5194/gmd-11-3681-2018, 2018.

Rodríguez-Fonseca, B., Mohino, E., Mechoso, C. R., Caminade, C., Biasutti, M., Gaetani, M., García-Serrano, J., Vizy, E. K., Cook, K., and Xue, Y.: Variability and predictability of West African droughts: a review on the role of sea surface temperature anomalies, Journal of Climate, 28, 4034–4060, https://doi.org/10.1175/JCLI-D-14-00130.1, 2015.

Rotstayn, L. D. and Lohmann, U.: Tropical Rainfall Trends and the Indirect Aerosol Effect, Journal of Climate, https://doi.org/10.1175/1520-0442(2002)015<2103:TRTATI>2.0.CO;2, 2002.

Ruprich-Robert, Y., Delworth, T., Msadek, R., Castruccio, F., Yeager, S., and Danabasoglu, G.: Impacts of the Atlantic Multidecadal Variability on North American Summer Climate and Heat Waves, Journal of Climate, https://doi.org/10.1175/JCLI-D-17-0270.1, 2018.

Ruprich-Robert, Y., Moreno-Chamarro, E., Levine, X., Bellucci, A., Cassou, C., Castruccio, F., Davini, P., Eade, R., Gastineau, G., Hermanson, L., Hodson, D., Lohmann, K., Lopez-Parages, J., Monerie, P.-A., Nicolì, D., Qasmi, S., Roberts, C. D., Sanchez-Gomez, E., Danabasoglu, G., Dunstone, N., Martin-Rey, M., Msadek, R., Robson, J., Smith, D., and Tourigny, E.: Impacts of Atlantic multidecadal variability on the tropical Pacific: a multi-model study, npj Climate and Atmospheric Science, 4, 1–11, https://doi.org/10.1038/s41612-021-00188-5, 2021.

Sanderson, B. M., Knutti, R., and Caldwell, P.: Addressing interdependency in a multimodel ensemble by interpolation of model properties, Journal of Climate, 28, 5150–5170, https://doi.org/https://doi.org/10.1175/JCLI-D-14-00361.1, 2015.

Sanogo, S., Fink, A. H., Omotosho, J. A., Ba, A., Redl, R., and Ermert, V.: Spatio-temporal characteristics of the recent rainfall recovery in West Africa, International Journal of Climatology, 35, 4589–4605, https://doi.org/10.1002/joc.4309, 2015.

Schneider, T., Bischoff, T., and Haug, G. H.: Migrations and dynamics of the intertropical convergence zone, nature, 513, 45–53, https://doi.org/10.1038/nature13636, 2014.

Schulzweida, U.: CDO User Guide, https://doi.org/10.5281/zenodo.10020800, 2023.

Shekhar, R. and Boos, W. R.: Improving Energy-Based Estimates of Monsoon Location in the Presence of Proximal Deserts, Journal of Climate, https://doi.org/10.1175/JCLI-D-15-0747.1, 2016.

Shekhar, R. and Boos, W. R.: Weakening and Shifting of the Saharan Shallow Meridional Circulation during Wet Years of the West African Monsoon, Journal of Climate, 30, 7399–7422, https://doi.org/10.1175/JCLI-D-16-0696.1, 2017.

Taylor, C. M., Belusic, D., Guichard, F., Arker, D. J. P., Vischel, T., Bock, O., Harris, P. P., Janicot, S., Klein, C., and Panthou, G.: Frequency of extreme Sahelian storms tripled since 1982 in satellite observations, Nature, 544, 475–478, https://doi.org/10.1038/nature22069, 2017.

Thorncroft, C. D., Nguyen, H., Zhang, C., and Peyrille, P.: Annual cycle of the West African monsoon: regional circulations and associated water vapour transport, Quarterly Journal of the Royal Meteorological Society, 137, 129–147, https://doi.org/10.1002/qj.728, 2011.

Ting, M., Kushnir, Y., Seager, R., and Li, C.: Robust features of Atlantic multi-decadal variability and its climate impacts, Geophysical Research Letters, 38, L17 705, https://doi.org/10.1029/2011GL048712, 2011.

Villamayor, J. and Mohino, E.: Robust Sahel drought due to the Interdecadal Pacific Oscillation in CMIP5 simulations, Geophysical Research Letters, 42, 1214–1222, https://doi.org/10.1002/2014GL062473, 2015.

https://doi.org/10.5194/egusphere-2026-382
Preprint. Discussion started: 29 January 2026

Villamayor, J., Mohino, E., Khodri, M., Mignot, J., and Janicot, S.: Atlantic Control of the Late Nineteenth-Century Sahel Humid Period, Journal of Climate, 31, 8225–8240, https://doi.org/10.1175/JCLI-D-18-0148.1, 2018.

Voldoire, A., Saint-Martin, D., Senesi, S., Decharme, B., Alias, A., Chevallier, M., Colin, J., Gueremy, J.-F., Michou, M., Moine, M.-P., Nabat, P., Roehrig, R., Salas y Melia, D., Seferian, R., Valcke, S., Beau, I., Belamari, S., Berthet, S., Cassou, C., Cattiaux, J., Deshayes, J., Douville, H., Ethe, C., Franchisteguy, L., Geoffroy, O., Levy, C., Madec, G., Meurdesoif, Y., Msadek, R., Ribes, A., Sanchez-Gomez, E., Terray, L., and Waldman, R.: Evaluation of CMIP6 DECK Experiments With CNRM-CM6-1, Journal of Advances in Modeling Earth Systems, 11, 2177–2213, https://doi.org/10.1029/2019MS001683, 2019.

Wang, C., Dong, S., Evan, A. T., Foltz, G. R., and Lee, S.-K.: Multidecadal covariability of North Atlantic sea surface temperature, African dust, Sahel rainfall, and Atlantic hurricanes, Journal of Climate, 25, 5404–5415, https://doi.org/10.1175/JCLI-D-11-00413.1, 2012.

Wang, G., Eltahir, E. A. B., Foley, J. A., Pollard, D., and Levis, S.: Decadal variability of rainfall in the Sahel: results from the coupled GENESIS-IBIS atmosphere-biosphere model, Climate Dynamics, 22, 625–637, https://doi.org/10.1007/s00382-004-0411-3, 2004.

Watanabe, M. and Tatebe, H.: Reconciling roles of sulphate aerosol forcing and internal variability in Atlantic multidecadal climate changes, Climate Dynamics, 53, 4651–4665, https://doi.org/10.1007/s00382-019-04811-3, 2019.

Williams, K. D., Copsey, D., Blockley, E. W., Bodas-Salcedo, A., Calvert, D., Comer, R., Davis, P., Graham, T., Hewitt, H. T., Hill, R., Hyder, P., Ineson, S., Johns, T. C., Keen, A. B., Lee, R. W., Megann, A., Milton, S. F., Rae, J. G. L., Roberts, M. J., Scaife, A. A., Schiemann, R., Storkey, D., Thorpe, L., Watterson, I. G., Walters, D. N., West, A., Wood, R. A., Woollings, T., and Xavier, P. K.: The Met Office Global Coupled Model 3.0 and 3.1 (GC3.0 and GC3.1) Configurations, Journal of Advances in Modeling Earth Systems, 10, 357–380, https://doi.org/10.1002/2017MS001115, 2018.

WMO, W. M. O.: Guide to Instruments and Methods of Observation. Volume I - Measurement of Meteorological Varibles, vol. WMO-No. 8, WMO, Geneva, Switzerland, ISBN 978-92-63-10008-5, https://library.wmo.int/idurl/4/41650, 2024.

Xue, J., Wang, B., Yu, Y., Li, J., Sun, C., and Mao, J.: Multidecadal variation of northern hemisphere summer monsoon forced by the SST inter-hemispheric dipole, Environmental Research Letters, 17, 044 033, https://doi.org/10.1088/1748-9326/ac5a65, 2022.

Zhang, J., Liu, Y., Sun, C., Li, J., Ding, R., Xie, F., Xie, T., Zhang, Y., and Gong, Z.: On the connection between AMOC and observed land precipitation in Northern Hemisphere: a comparison of the AMOC indicators, Climate Dynamics, 56, 651–664, https://doi.org/10.1007/s00382-020-05496-9, 2021.

Zhang, R. and Delworth, T. L.: Impact of Atlantic multidecadal oscillations on India/Sahel rainfall and Atlantic hurricanes, Geophysical Research Letters, 33, L17 712, https://doi.org/10.1029/2006GL026267, 2006.

Zhang, R., Sutton, R., Danabasoglu, G., Kwon, Y.-O., Marsh, R., Yeager, S. G., Amrhein, D. E., and Little, C. M.: A Review of the Role of the Atlantic Meridional Overturning Circulation in Atlantic Multidecadal Variability and Associated Climate Impacts, Reviews of Geophysics, 57, 316–375, https://doi.org/10.1029/2019RG000644, 2019.

Zhang, S., Stier, P., Dagan, G., and Wang, M.: Anthropogenic Aerosols Modulated 20th-Century Sahel Rainfall Variability Via Their Impacts on North Atlantic Sea Surface Temperature, Geophysical Research Letters, 49, e2021GL095 629, https://doi.org/10.1029/2021GL095629, 2022.

https://doi.org/10.5194/egusphere-2026-382
Preprint. Discussion started: 29 January 2026

Table 1. Overview of the different models used in this study, together with approximate horizontal resolution, number of atmospheric vertical levels, protocol followed for the simulations, number of members for each experiment, and main reference for the model documentation

Model	Atmospheric horizontal resolution	Number of atmospheric vertical levels)	Protocol	Members	Reference
IPSL-CM6A-LR	2.5° × 1.3°	79	DCPP-C	50	Boucher et al. (2020)
CNRM-CM6-1	1.4° × 1.4°	91	DCPP-C	26	Voldoire et al. (2019)
EC-Earth3*	∼ 100 km	91	DCPP-C	32	Döscher et al. (2022)
HadGEM3-GC31-MM†	0.83° × 0.55°	85	DCPP-C	25	Williams et al. (2018)
CNRM-CM6-1	1.4° × 1.4°	91	PRIMAVERA	15	Voldoire et al. (2019)
EC-Earth3P-HR	∼ 50 km	91	PRIMAVERA	17	Haarsma et al. (2020)
EC-Earth3P†	∼ 100 km	91	PRIMAVERA	25	Haarsma et al. (2020)
ECMWF-IFS-HR‡	∼ 25 km	91	PRIMAVERA	15	Roberts et al. (2018)
ECMWF-IFS-LR‡	∼ 50 km	91	PRIMAVERA	30	Roberts et al. (2018)
MetUM-GOML2-HR	0.83° × 0.55°	85	PRIMAVERA	15	Hirons et al. (2015)
MetUM-GOML2-LR	1.875° × 1.25°	85	PRIMAVERA	15	Hirons et al. (2015)
MPI-ESM1-2-HR§	∼ 100 km	95	PRIMAVERA	10	Gutjahr et al. (2019)
MPI-ESM1-2-XR§	∼ 50 km	95	PRIMAVERA	10	Gutjahr et al. (2019)

* Too few vertical levels were available in the output of this model, so it was excluded from both the vertical profile analysis and the calculation of low-level atmospheric thickness.

† No soil moisture data was available for these models.

‡ No near-surface specific humidity data was available for these models.

§ Due to an unrealistic response (see section 3.1), these models are removed from the results shown in the paper. Note that this does not affect the main conclusions of the manuscript.

https://doi.org/10.5194/egusphere-2026-382
Preprint. Discussion started: 29 January 2026

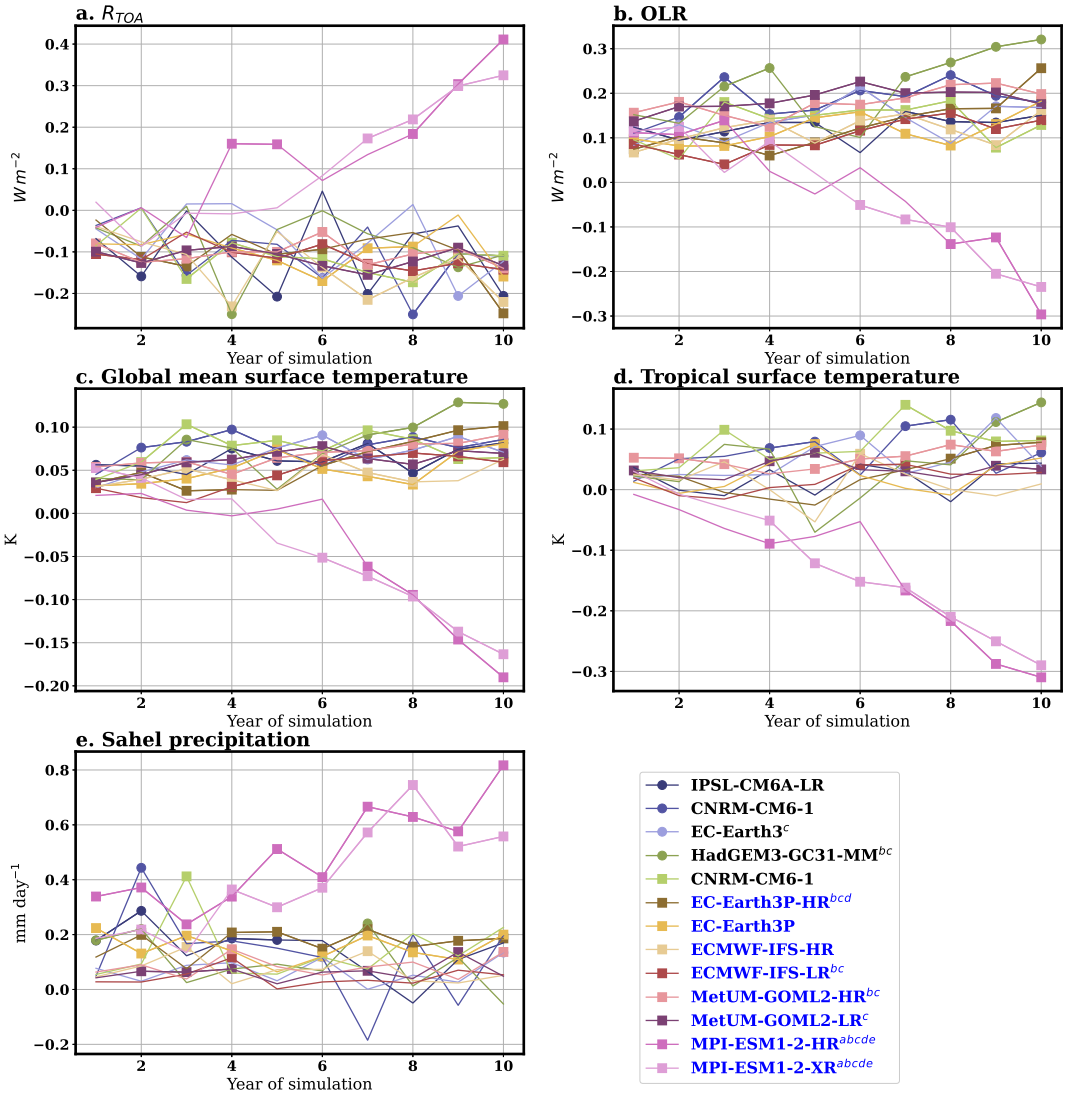

Figure 1. Simulation drifts. Differences between AMV^{+} and AMV^{-} yearly means averaged across all ensemble members for each model vs simulated year for: a) global mean net TOA energy imbalance R_{TOA} (W m^{-2}); b) global mean OLR (W m^{-2}, positive anomalies meaning the Earth is loosing more longwave radiation at TOA in AMV^{+} than in AMV^{-}); c) global mean surface temperature (K); d) tropical (20ºS–20ºN) mean surface temperature (K); e) Sahel rainfall (averaged over the 10ºW–10ºE, 10ºN–20ºN box, mm day^{-1}). For the models following the PRIMAVERA protocol (marked as blue in the model names), only half the anomalies are shown. Solid symbols mark statistically significant differences (two-tailed t-test) in the AMV^{+} and AMV^{-} experiments evaluated separately for each year. Letters a to e next to the model name indicate trends in the variables shown in the corresponding plot that are statistically different from 0 (at the level of $\alpha = 0.05$).

https://doi.org/10.5194/egusphere-2026-382
Preprint. Discussion started: 29 January 2026

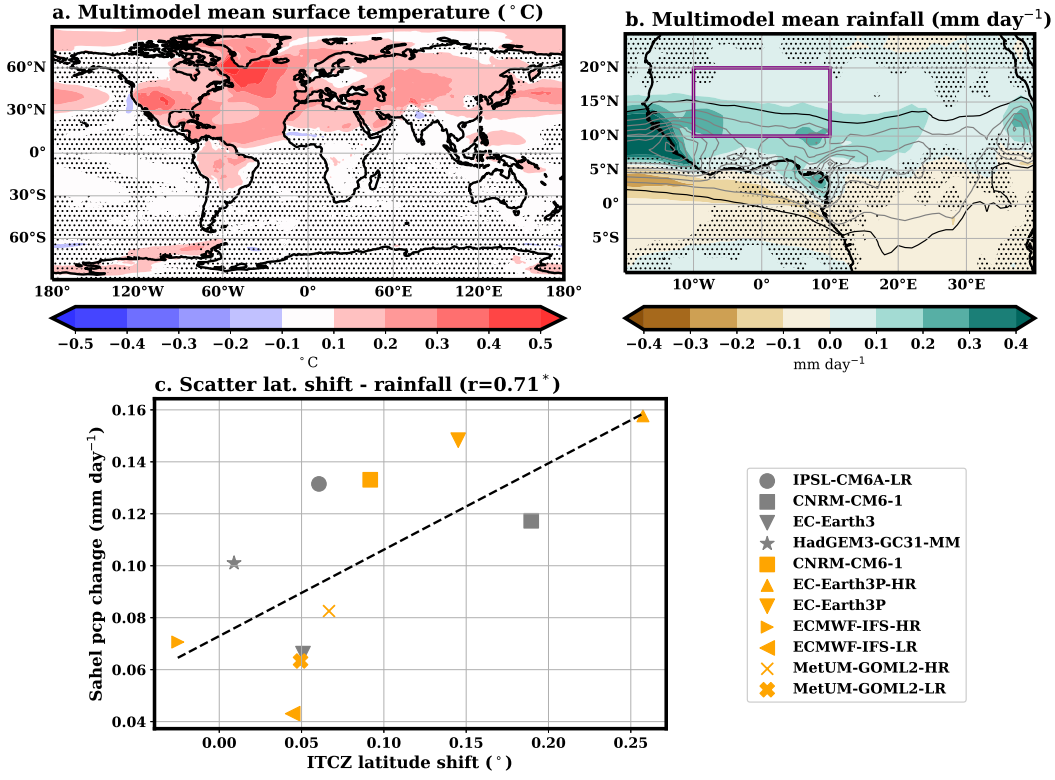

Figure 2. Multimodel mean AMV$^+$ minus AMV$^-$ change in JAS for: (a) surface temperature (°C) and (b) rainfall over West Africa ($\mathrm{mm\,day^{-1}}$). Dots mark regions where less than 80% of the models (less than 9 out of 11) agree on the sign of changes. Contours in plot b show multimodel mean JAS rainfall (grey contours are drawn every 2 $\mathrm{mm\,day^{-1}}$ with the starting black contour at 2 $\mathrm{mm\,day^{-1}}$). c) Scatter of Sahel (10ºW–10ºE, 10ºN–20ºN, see purple box in plot b) rainfall change as a function of the ITCZ latitude shift (°) averaged over the 10ºW–10ºE longitude range. The dashed line shows the linear regression fit, and the correlation coefficient is shown in the title. Correlations are marked with one asterisk if they are statistically significant at the level of α=0.05 when taking all the models as independent samples. Two asterisks are used if correlations are statistically significant when lowering the number of independent samples to 6. For the models following the PRIMAVERA protocol (marked with orange symbols in the scatter plot), only half the anomalies are shown.

https://doi.org/10.5194/egusphere-2026-382
Preprint. Discussion started: 29 January 2026

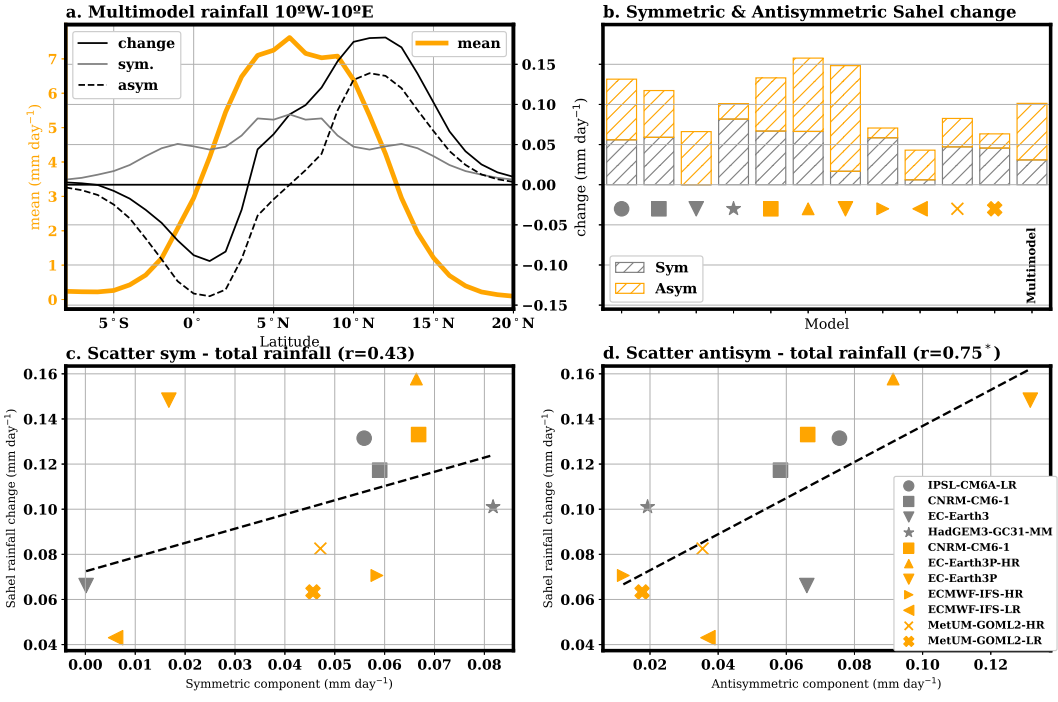

Figure 3. Decomposition of rainfall changes into symmetric and antisymmetric components. a) Multimodel mean climatology of rainfall in JAS averaged between 10ºW and 10ºE (orange, left axis, $\mathrm{mm\,day^{-1}}$) and AMV$^+$ minus AMV$^-$ change (black continuous line, right axis, $\mathrm{mm\,day^{-1}}$). The change has been decomposed into symmetric (grey line, right axis) and antisymmetric (dashed line, right axis), relative to the maximum climatological value. b) Symmetric and antisymmetric components of AMV$^+$ minus AMV$^-$ average rainfall change in the Sahel box (see purple box in Fig. 2b) in JAS for all models and the multimodel mean ($\mathrm{mm\,day^{-1}}$). c and d) show scatter plots of rainfall change in the Sahel box as a function of its symmetric and antisymmetric components, respectively ($\mathrm{mm\,day^{-1}}$). For the models following the PRIMAVERA protocol (marked as orange symbols), only half the anomalies are shown. In the scatter plots, the dashed line shows the linear regression fit, and the correlation coefficient is shown in the title. Correlations are marked with one asterisk if they are statistically significant at the level of α=0.05 when taking all the models as independent samples. Two asterisks are used if correlations are statistically significant when lowering the number of independent samples to 6.

https://doi.org/10.5194/egusphere-2026-382
Preprint. Discussion started: 29 January 2026

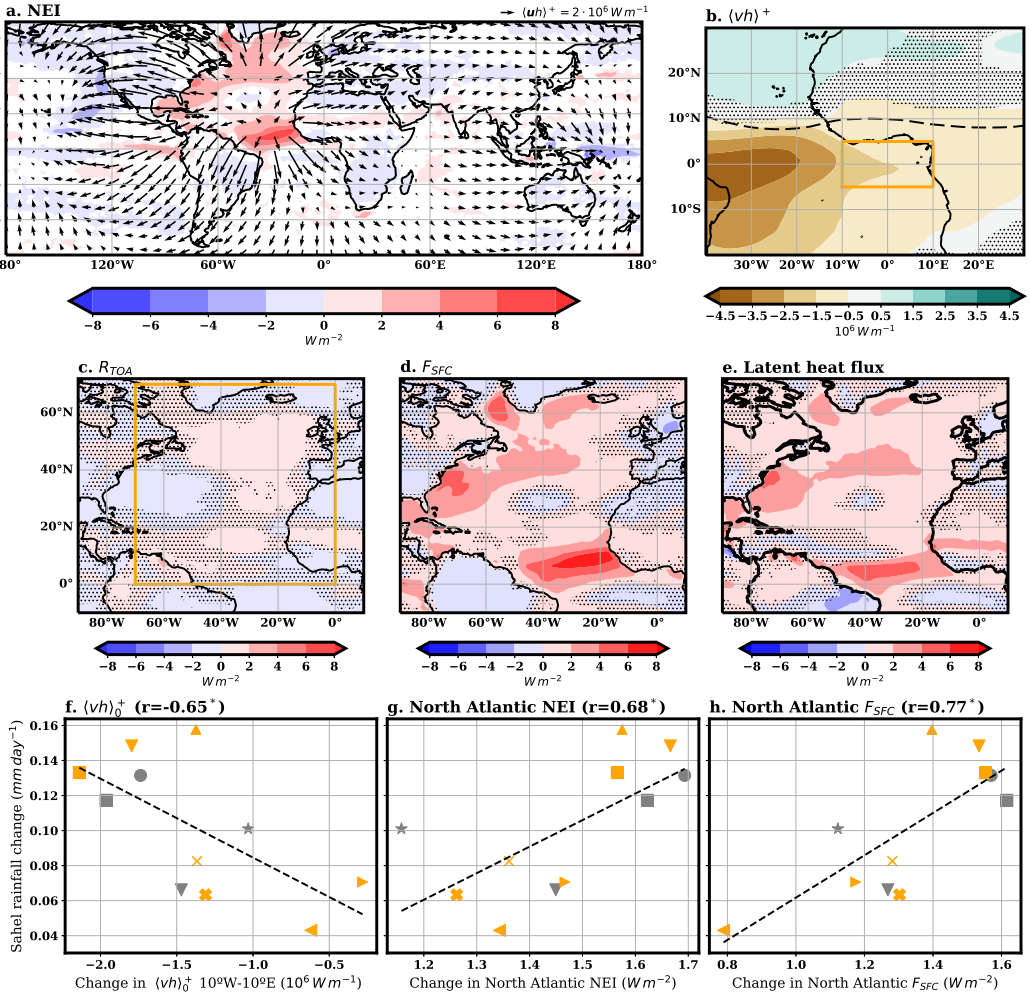

Figure 4. Multimodel average changes in AMV$^+$ minus AMV$^-$ in JAS for: a) net energy input (NEI) into the atmospheric column (W m^{-2}, shaded) and associated divergent component of the column integrated MSE flux ($\langle \boldsymbol{u}h \rangle^+$, 10^6W m^{-1}, arrows); b) meridional component of the divergent column integrated MSE flux ($\langle vh \rangle^+$, with v meridional wind, 10^6W m^{-1}); c) energy imbalance at TOA (R_{TOA}, W m^{-2}); d) energy imbalance at the surface (F_{SFC}, W m^{-2}); e) latent heat flux at surface (W m^{-2}). For the NEI and the energy imbalances, positive values indicate energy gain for the atmosphere. Scatter plots of averaged Sahel rainfall change (mm day^{-1}) and: f) strength of the meridional component of the divergent column integrated MSE flux at equatorial latitudes averaged over the Sahel longitudes ($\langle vh \rangle_0^+$, 10^6W m^{-1}, see orange box in plot b); g) NEI averaged over the North Atlantic (W m^{-2}, see orange box in plot c); h) surface energy imbalance averaged over the North Atlantic (F_{SFC}, W m^{-2}). For plot a, anomalies are only shown in regions where at least 80% (9 out of 11) of simulations agree on their sign. Dots in plots b, c, d, and e mark regions where fewer than 80% of the models agree on the sign of changes. For the models following the PRIMAVERA protocol (marked with orange symbols in the scatter plot), only half the anomalies are shown. The legend for the symbols in the scatter plots is the same as in Fig. 2c. In the scatter plots, the dashed line shows the linear regression fit, and the correlation coefficient is shown in the title. Correlations are marked with one asterisk if they are statistically significant at the α= 0.05 level when considering all models as independent samples. Two asterisks are used if correlations are statistically significant when lowering the number of independent samples to 6.

https://doi.org/10.5194/egusphere-2026-382
Preprint. Discussion started: 29 January 2026

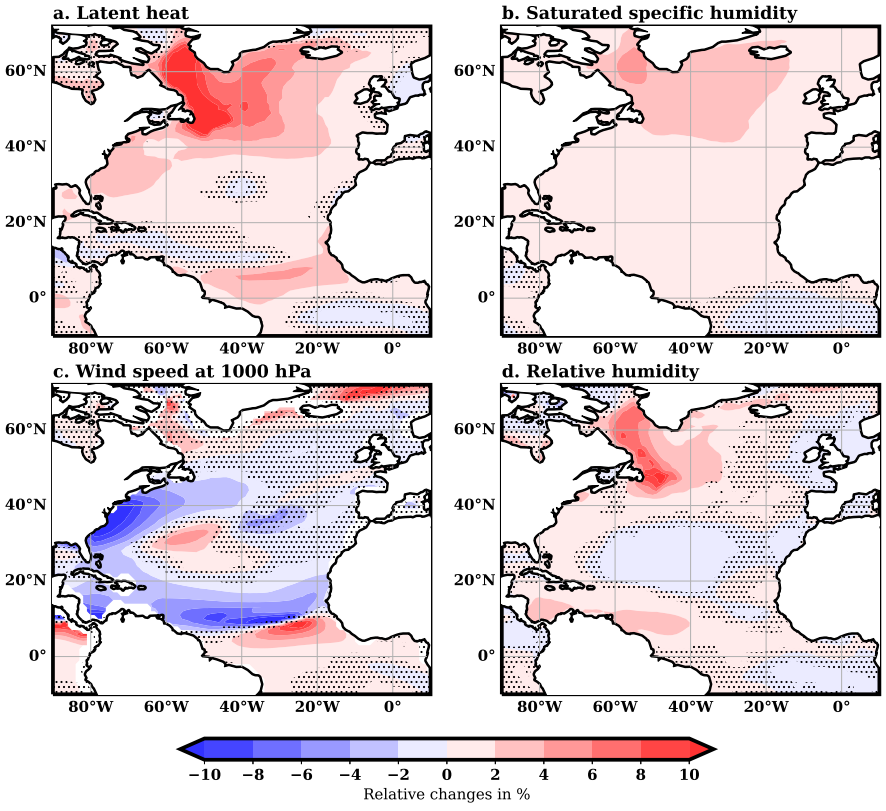

Figure 5. Multimodel averaged relative changes in AMV$^+$ minus AMV$^-$ in JAS for: a) latent heat; b) saturation specific humidity at surface; c) wind speed at 1000 hPa; and d) near-surface relative humidity (plotted as $-\delta RH/(1-\overline{RH})$). Relative humidity is calculated using near-surface specific humidity and the saturated specific humidity at the surface. The latter is estimated over the ocean by first calculating the saturated vapour pressure based on surface temperature (WMO, 2024) and then transforming it into saturation specific humidity, taking into account sea level pressure. Note that ECMWF-IFS-HR and ECMWF-IFS-LR models were not used for surface calculations since they did not provide near-surface specific humidity. Likewise, EC-Earth3 was not used for wind speed at 1000 hPa. Changes are relative to the climatological values at each grid point, which are calculated as half the sum of AMV$^+$ and AMV$^-$ simulations. Dots mark regions where fewer than 80% of the models agree on the sign of changes, and values over land are masked out.

https://doi.org/10.5194/egusphere-2026-382
Preprint. Discussion started: 29 January 2026

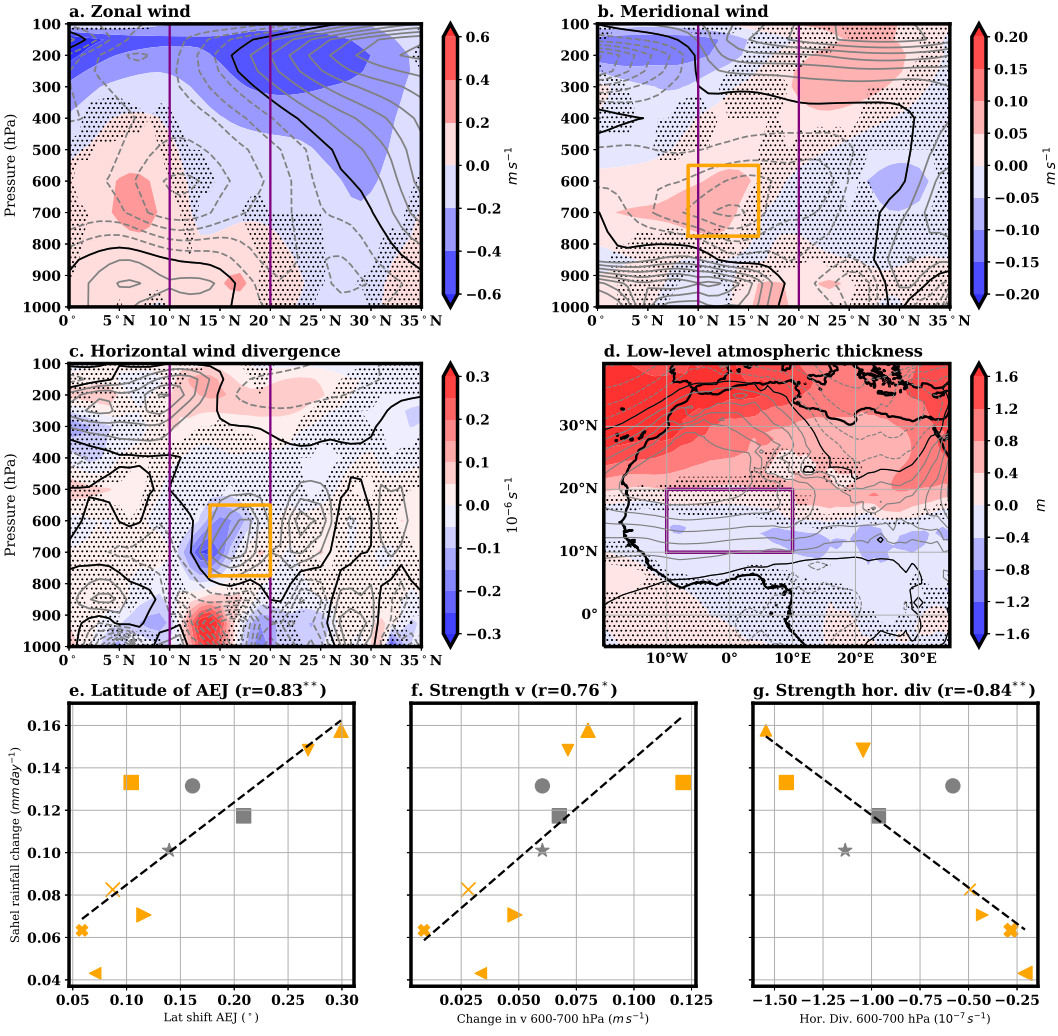

Figure 6. Multimodel average changes (shaded) in AMV^{+} minus AMV^{-} in JAS and climatological values (gray contours, solid for positive values and dashed for negative ones, black contours mark zero isoline) of: a) zonal wind averaged between 10ºW and 10ºE ($\mathrm{m \cdot s^{-1}}$, contours drawn every 2 $\mathrm{m \cdot s^{-1}}$); b) meridional wind averaged between 10ºW and 10ºE ($\mathrm{m \cdot s^{-1}}$, contours drawn every 0.5 $\mathrm{m \cdot s^{-1}}$); c) divergence of horizontal wind averaged between 10ºW and 10ºE (10^{-6} $\mathrm{s^{-1}}$, contours drawn every 10^{-6} $\mathrm{s^{-1}}$); d) low-level atmospheric thickness with respect to average tropical values (m, contours drawn every 10 m). Purple vertical lines in plots a, b and c mark the Sahel latitudes. Scatter plots of rainfall change ($\mathrm{mm \cdot day^{-1}}$) averaged over the Sahel box (10ºW–10ºE, 10ºN–20ºN, see purple box in plot d) and: e) the shift in the latitude of AEJ (°); f) the change in the northerly meridional wind ($\mathrm{m \cdot s^{-1}}$) averaged in the 10ºW-10ºE, 9ºN-16ºN box and between 600 and 700 hPa pressure levels (see orange box in plot b); g) the change in strength of the horizontal wind divergence (10^{-6} $\mathrm{s^{-1}}$) averaged in the 10ºW-10ºE, 14ºN-20ºN box and between 600 and 700 hPa pressure levels (see orange box in plot c). For the models following the PRIMAVERA protocol (marked with orange symbols in the scatter plot), only half of the anomalies are shown. The legend for the symbols in the scatter plots is the same as in Fig. 2c. In the scatter plots, the dashed line shows the linear regression fit, and the correlation coefficient is shown in the title. Correlations are marked with one asterisk if they are statistically significant at the α=0.05 level when considering all models as independent samples. Two asterisks are used if correlations are statistically significant when lowering the number of independent samples to 6.

https://doi.org/10.5194/egusphere-2026-382
Preprint. Discussion started: 29 January 2026

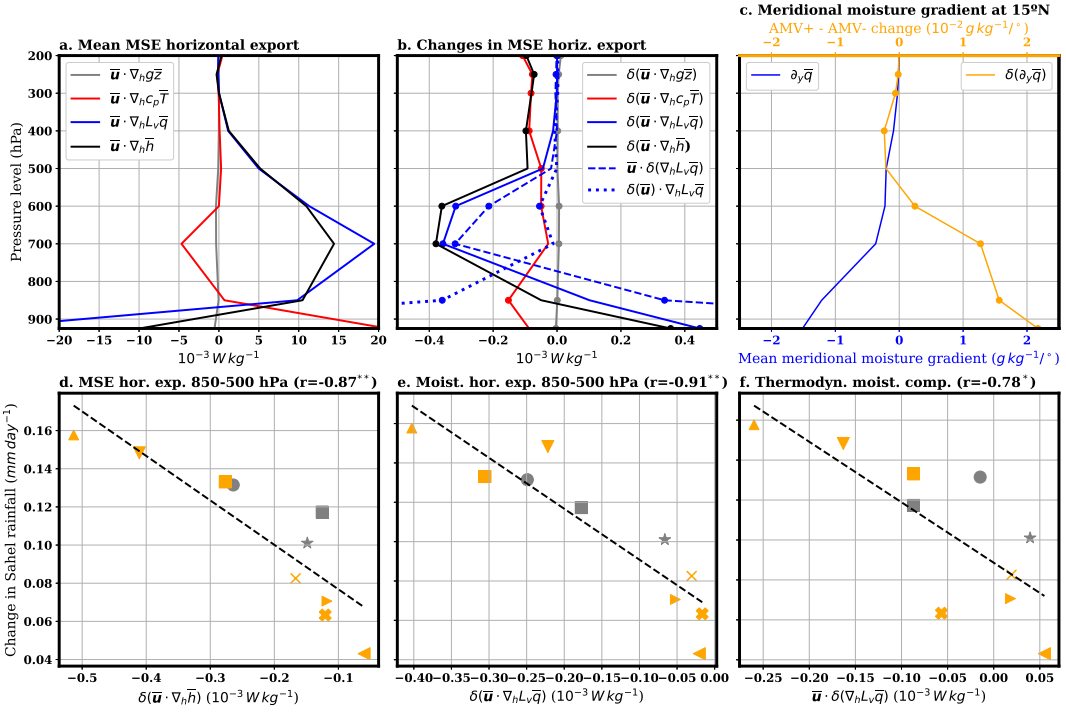

Figure 7. a) Climatological export of MSE by the time-mean horizontal flow ($\overline{\boldsymbol{u}}\nabla_h\overline{h}$, black line) partitioned into the potential energy ($\overline{\boldsymbol{u}}\nabla_h g\overline{z}$, grey line), sensible ($\overline{\boldsymbol{u}}\nabla_h c_p\overline{T}$, red line), and latent enthalpy ($\overline{\boldsymbol{u}}\nabla_h L_v\overline{q}$, blue line) components averaged over the Sahel box (10ºW-10ºE, 10ºN-20ºN) for the multimodel mean. b) AMV$^+$ minus AMV$^-$ multimodel change in the export of MSE by the time-mean horizontal flow ($\delta(\overline{\boldsymbol{u}}\nabla_h\overline{h})$, black) partitioned into the potential energy ($\delta(\overline{\boldsymbol{u}}\nabla_h g\overline{z})$, grey), sensible ($\delta(\overline{\boldsymbol{u}}\nabla_h c_p\overline{T})$, red), and latent enthalpy ($\delta(\overline{\boldsymbol{u}}\nabla_h L_v\overline{q})$, blue) averaged over the Sahel box. The change in latent enthalpy has been further decomposed into its thermodynamic ($\overline{\boldsymbol{u}}\delta(\nabla_h L_v\overline{q})$, blue dashed) and dynamic ($\delta(\overline{\boldsymbol{u}})\nabla_h L_v\overline{q}$, blue dotted) components. c) Multimodel mean meridional gradient of the 10ºW-10ºE zonally averaged specific humidity ($g\,kg^{-1}$ per $^{\circ}$) at 15ºN ($\partial_y\overline{q}$, blue) and AMV$^+$ minus AMV$^-$ changes ($\delta(\partial_y\overline{q})$, orange). Scatter plots of averaged Sahel rainfall change ($mm\,day^{-1}$) and averages of changes over the Sahel box between 850 hPa and the 500 hPa levels of: d) total export of MSE due to time-mean horizontal flow ($\delta(\overline{\boldsymbol{u}}\nabla_h\overline{h})$); e) MSE export due to horizontal moisture advection in MSE units ($\delta(\overline{\boldsymbol{u}}\nabla_h L_v\overline{q})$); and f) its thermodynamic component also in MSE units ($\overline{\boldsymbol{u}}\delta(\nabla_h L_v\overline{q})$). Units for the energetic terms are 10^{-3} W kg^{-1}. For the models following the PRIMAVERA protocol (marked with orange symbols), only half of the anomalies are shown. The legend for the symbols in the scatter plots is the same as in Fig. 2c. Dots in plots b and c mark changes for which at least 80 % of the models agree on the sign. In the scatter plots, the dashed line shows the linear regression fit, and the correlation coefficient is shown in the title. Correlations are marked with one asterisk if they are statistically significant at the level of α=0.05 when taking all the models as independent samples. Two asterisks are used if correlations are statistically significant when lowering the number of independent samples to 6.